Available online at www.sciencedirect.com
SCIENCE DIRECT®
Remote Sensing of Environment 86 (2003) 83–107
Remote Sensing of Environment
www.elsevier.com/locate/rse

Fire radiative energy for quantitative study of biomass burning: derivation from the BIRD experimental satellite and comparison to MODIS fire products

M.J. Wooster[a,*], B. Zhukov[b,1], D. Oertel[b,1]

[a] *Department of Geography, King's College London, Strand, London WC2R 2LS, UK*
[b] *Institute of Space Sensor Technology and Planetary Exploration, Rutherfordstr. 2, D-12489 Berlin, Germany*

Received 30 July 2002; received in revised form 27 February 2003; accepted 9 March 2003

Abstract

A major focus in global change research is to quantify the amount of gaseous and particulate pollutants emitted from terrestrial vegetation fires. Determination of the emitted radiant energy released during biomass combustion episodes (the so-called fire radiative energy or FRE) has been suggested as a new tool for determining variations in biomass combustion rates and the rate of production of atmospheric pollutants. We review the physical principals behind the remote determination of FRE and present an alternative method for its derivation via analysis of 'fire pixel' radiances in the middle infrared spectral region. We compare our method to the existing FRE retrieval approach used in the EOS Moderate Resolution Imaging Spectro-radiometer (MODIS) fire products, and to retrievals of FRE based on derived fire temperature and area made via the so-called Bi-spectral method. We test each FRE retrieval method using both simulated data and imagery from a new experimental space mission, the Bi-spectral InfraRed Detection (BIRD) small satellite, which has sensors specifically designed for the study of active fires. We analyse near simultaneous MODIS and BIRD data of the fires that burned around Sydney, Australia in January 2002. Despite the markedly different pixel size and spectral coverage of these sensors, where the spatial extent of the fire pixel groups detected by MODIS and BIRD are similar, the derived values of FRE for these fires agree to within ± 15 %. However, in certain fires, the lower spatial resolution of MODIS appears to prevent many of the less intensely radiating fire pixels being detected as such, meaning MODIS underestimates FRE for these fires by up to 46% in comparison to BIRD. Though the FRE release of each of these low intensity fire pixels is relatively low, their comparatively large number makes their overall FRE significant. Thus, total FRE release of the Sydney fires on 5 January 2002 is estimated to be 6.5×10^9 J s^{-1} via BIRD but 4.0×10^9 J s^{-1} via MODIS. The ability of BIRD to resolve individual fire fronts further allows the first accurate calculation of 'radiative' fireline intensity from spaceborne measurements, providing values of 15–75 kJ s^{-1} m^{-1} for fire fronts that are up to 9 km in length. Finally, we analyse the effectiveness of the satellite-based FRE retrieval methods in estimating the FRE from the active flaming and smouldering components only (FRE_{Active}, believed to be proportional to the rate of biomass combustion), despite the sensor receiving additional radiance from the 'cooling ground'. The MIR radiance method appears particularly strong in this regard, allowing FRE_{Active} to be estimated to within ± 30% in the range 100–100,000 J s^{-1} m^{-2}. These results provide further confidence in the ability of spaceborne missions to derive physically meaningful values of FRE that could be used to support biomass burning emissions inventories. Future comparisons between FRE derived via MODIS and those from higher spatial resolution BIRD or airborne imagery may allow the MODIS-derived FRE values to be 'calibrated' for any systematic underestimation. We therefore expect FRE to become an important tool for enhancing global studies of terrestrial vegetation fires with infrared remote sensing, particularly as the majority of large fires are now imaged four times per day via the MODIS instruments on the Terra and Aqua spacecraft.

Keywords: Biomass burning; Infrared; Fires; Fire radiative energy; BIRD; MODIS

1. Introduction

The worldwide combustion of forest and grassland vegetation releases large volumes of radiatively active gases, pyrogenic aerosols, and other chemically active species that significantly influence Earth's radiative budget and atmospheric chemistry (Andreae & Merlet, 2001).

* Corresponding author. Fax: +44-207-8482287.
E-mail addresses: martin.wooster@kcl.ac.uk (M.J. Wooster), Boris.Zhukov@dlr.de (B. Zhukov), Dieter.Oertel@dlr.de (D. Oertel).
[1] Fax: +49-30-67055-565.

0034-4257/03/$ - see front matter © 2003 Elsevier Science Inc. All rights reserved.
doi:10.1016/S0034-4257(03)00070-1

Scholes and Andreae (2000) have recently estimated that around 9200 Tg ± 50% (dry weight) of terrestrial vegetation is combusted per year, but improved data on regional and interannual variations is required to fully investigate the specific emissions sources and their subsequent transportation and effect (Wittenberg, Heimann, Esser, McGuire, & Sauf, 1998). This requirement has led to pyrogenic emissions estimation becoming a major research focus in the global change community, particularly so because of the need to better understand the effects of these emissions on the global climate (Crutzen & Andreae, 1990; Scholes & Andreae, 2000). A few studies such as Kaufman, Tucker, and Fung (1990) and Spichtinger et al. (2001) have directly analysed emissions of smoke or particular chemical species via satellite sensor observations. However, the majority of pyrogenic emissions inventories are derived via relationships linking the concentrations of pollutant products to the amount of biomass combusted, the latter being commonly estimated from historical information on fire-frequency or from fire counts or maps of 'burn-scars' derived from Earth observation imagery (Andreae & Merlet, 2001). These data sources provide important information relating to burned area, but converting such measurements into estimates of burnt biomass involves additional knowledge of the pre-burn biomass density and the combustion factor (essentially the fraction of available biomass actually burnt). For the large areas affected by biomass burning, these factors are difficult or impossible to measure on the ground, but are also problematic to measure remotely (Pereira et al., 1999). Hence, biomass combustion and pyrogenic emissions estimates are often subject to potentially large errors. Andreae and Merlet (2001) demonstrate the current level of uncertainty by comparing emissions estimates for the savanna regions of southern African, based on both the traditional fire-frequency and current Earth observation approaches. Results from the two techniques differ by an order of magnitude, leading Andreae and Merlet to conclude that new and independent routes for providing pyrogenic emissions estimates are urgently required to resolve these differences and to improve regional and global assessments.

To address the requirement for new remote sensing tools useful for the estimation of biomass combustion rates and the associated emissions, Kaufman et al. (1996) introduced the concept of remotely measured fire radiative energy (FRE). Terrestrial, airborne, and spaceborne remote sensing has long been used to provide data on 'fire counts', essentially by detecting the strong infrared thermal emission signal associated with active fires (e.g., Hirsch, Kruckeberg, & Madden, 1971; Matson, Schneider, Aldridge, & Satchwell, 1984; Waggoner, 1991). However, the enhancement proposed by Kaufman et al. was that quantification of the amount of energy radiated during the combustion process could provide a remote measurement related directly to the fire intensity and the amount of vegetation consumed per unit time. Remotely sensed FRE is therefore a candidate for the independent emissions-estimation route called for by Andreae and Merlet (2001). Kaufman et al. introduced the FRE concept for use with the Moderate Resolution Imaging Spectro-radiometer (MODIS), launched on the Terra and Aqua satellites in December 1999 and May 2002, respectively; this being possible due to the inclusion of low-gain infrared channels on MODIS that, unlike those on previous satellite imagers, provides unsaturated infrared measurements over even the largest fires. Kaufman, Justice, et al. (1998) and Kaufman, Kleidman, and King (1998) first used the method with data from the MODIS Airborne Simulator and reported the encouraging result that time-integrated FRE was better related to the observed growth of burnt areas than was a simple count of active fire pixels. Recently, Wooster (2002) quantitatively tested the relationship between FRE and the amount of biomass combusted using field spectro-radiometer observations of small experimental burns. Over almost two orders of magnitude the results show a linear agreement ($r^2 = 0.76$, $n = 12$) between the total radiative energy emitted during the burn (so-called time-integrated FRE) and the mass of vegetation combusted. We believe these results strongly support the idea of FRE as a valuable addition to the array of techniques used to assess biomass combustion in natural wildfires.

There are some limitations, however, not least the issue of cloud-cover that will obstruct satellite-derived FRE observations. There is also the issue that during combustion energy is lost by a variety of processes in addition to radiation, such as convection of the airmass above the fire and conduction into the ground (Asensio & Ferragut, 2002). However, the high temperatures involved in vegetation fires means that radiant energy loss is intense and the early studies cited above suggest that FRE is a valuable addition to the tools used to inform studies of biomass burning and the production and transport of atmospheric pollutants. Furthermore, its determination via spaceborne remote sensing means it can be derived on a subdaily basis for all regions subject to large-scale vegetation fire activity, cloud-cover permitting. In the current paper, we explain further the physical principals behind the remote measurement of FRE and present a new algorithm for its derivation, which we compare to existing approaches. We apply the differing FRE-derivation techniques to simulated observations and to real data from a newly launched spaceborne mission, the Bi-spectral InfraRed Detection (BIRD) small satellite, analysing the benefits and limitations of each approach. BIRD has been specifically designed to target high temperature events such as active fires, and the BIRD Hot Spot Recognition System (HSRS) operates with a 370-m pixel size compared to the 1–4-km pixel size of existing sensors most commonly used to study fire (Fuller, 2000; Robinson, 1991). As such, in addition to providing important data in its own right, BIRD is expected to play an important role in validating lower spatial resolution fire products such as those from the AVHRR, ATSR, AATSR, GOES, and MODIS space missions. We provide the first comparison of near-simultaneous FRE observations of natural fires

made from spaceborne sensors having markedly different characteristics, namely the BIRD-HSRS and Terra-MODIS instruments. The targets are the intense fires that burned around Sydney, Australia in January 2002. Finally, we analyse the effectiveness of the satellite-based FRE retrieval methods in estimating FRE from the active fire (flaming and smouldering) components only, believed to be the quantity most likely to be proportional to the rate of biomass combustion, despite the sensor recording an additional radiance contribution from the cooling ground that has recently been heated by the fires passage.

2. The BIRD small satellite

Fig. 1 shows the BIRD satellite during pre-launch testing. On 22 October 2001, the satellite was successfully piggy-back launched into a circular, sun-synchronous 572 km orbit using an Indian Polar Satellite Launch Vehicle (PSLV-C3) (Briess et al., 2002). The BIRD imaging payload consists of the HSRS and a Wide-Angle Optoelectronic Stereo Scanner (WAOSS-B). HSRS possesses a mid-infrared band (MIR, centred at 3.8 μm) and a thermal infrared band (TIR, centred at 8.9 μm), whilst WAOSS-B possesses a nadir-looking near-infrared band (NIR, centred at 0.87 μm) and two off-nadir stereo channels (visible and NIR, centred at 0.635 and 0.87 μm, respectively). Further detail on the HSRS and WAOSS-B sensors is provided in Table 1.

Fig. 1. The BIRD satellite during the test cycle at DLR Institute of Space Sensor Technology and Planetary Exploration (Berlin). The satellites two imaging sensors, WAOSS-B and HSRS, are located in the satellites upper compartment, with their entrance apertures facing forward in the picture. The optical WAOSS-B sensor entrances (upper left) are uncovered, but the two HSRS infrared sensor entrances (upper right) are shown closed by the rear sides of the calibration units, which are covered in multilayer isolation.

Table 1
Characteristics of the BIRD main sensor payload

	HSRS	WAOSS-B
Spectral bands	MIR: 3.4–4.2 μm TIR: 8.5–9.3 μm	VIS: 0.60–0.67 μm NIR: 0.84–0.90 μm
Focal length	46.39 mm	21.65 mm
Field of view	19°	50°
f-number	2.0	2.8
Detector type	CdHgTe arrays	CCD lines
Detector cooling	Stirling, 80–100 K	Passive, 293 K
Pixel size	30 × 30 μm	7 × 7 μm
Pixel number	2 × 512 staggered	2880
Quantisation	14 bit (for each exposure)	11 bit
Ground pixel size	370 m	185 m
Sampling step	185 m	185 m
Swath width	190 km	533 km

Note that BIRD HSRS pixels are oversampled by a factor of 2 in the along and across-track directions.

The BIRD-HSRS has been specifically designed to support hotspot detection and the analysis of infrared radiation emitted from active fires and volcanoes. The HSRS detectors consist of two Cadmium Mercury Telluride (CdHgTe) linear photodiode arrays of 512 elements, arranged in a staggered structure parallel to one other, with an along-line shift of half the detector element size. Data from the HSRS sensor are read out continuously, with a sampling interval that is exactly one half of the pixel dwell time. This precise double sampling, coupled with the staggered line array structure, provides a sampling step coincident with that of the WAOSS NIR nadir channel, which is two times smaller than the HRSR pixel size (Skrbek & Lorenz, 1998). Real-time processing of HSRS data is carried out onboard the satellite, and if this processing indicates that detector elements are saturated, or close to saturation, in the first exposure then a second exposure is performed with a reduced integration time (but still within the same sampling interval). This results in an effective HSRS dynamic range that eliminates detector saturation over high temperature targets but which preserves a 0.1–0.2 K radiometric resolution at ambient temperature pixels (Lorenz & Skrbek, in press). This level of radiometric precision is required for the accurate estimation of the infrared background temperature at ambient pixels surrounding any detected ‘fire’ pixel, which is a requirement for accurate application of the Bi-spectral method for fire size and temperature determination, as discussed in Section 4.1 (Dozier, 1981; Giglio & Kendall, 2001). As with the BIRD-HSRS system, the EOS MODIS sensor is also required to provide both unsaturated infrared data of hot targets and a high radiometric precision over ambient temperature surfaces. However, MODIS accomplishes this by having two separate channels in the same MIR spectral band of interest (Kaufman, Justice, et al., 1998), one low gain (band 21) to provide unsaturated observations (NEdT 2 K, saturation ~ 450 K), and one standard-gain (band 22) to provide high radiometric precision (NEdT 0.07 K, saturation 335 K).

3. Fire radiative energy

3.1. FRE background

Fire radiative energy is essentially the portion of the chemical energy liberated from burning vegetation and emitted as radiation during the process of combustion. Infrared spectro-radiometers, such as those present on Earth-orbiting satellites, can directly measure this emitted thermal radiation. However, when observing active fires from Earth orbit the ground footprint of each 'fire pixel' will usually be far from homogeneous and can be considered to comprise n thermal components, each having a different temperature and subpixel area. Depending upon the exact pixel size, both lower temperature cooling–smouldering activity and higher temperature flaming activity may be present within the same ground pixel (Robinson, 1991). For each hotspot pixel, total FRE from all fire thermal components (not including the ambient background) can be calculated as:

$$\mathrm{FRE}_{\mathrm{TRUE}} = A_{\mathrm{sampl}}\varepsilon\sigma\sum_{i=1}^{n} A_n T_n^4 \quad (1)$$

where: $\mathrm{FRE}_{\mathrm{TRUE}}$ = fire radiative energy (J s^{-1}), A_{sampl} = ground sampling area (m^2), σ = Stefan–Boltzmann constant (5.67×10^{-8} J s^{-1} m^{-2} K^{-4}), A_n = fractional area of nth surface thermal component within the individual ground pixel, T_n = temperature of the nth thermal component (K), ε = emissivity, a composite value depending on the mixing ratio of flaming and smouldering combustion. Fires are assumed to radiate as grey bodies, an assumption that maybe updated if more accurate flame emissivity data become available (Langaas, 1995). The emissivity of smouldering and cooling ground and optically thick flames may approach one, but small fires will likely have a somewhat lower emissivity.

Eq. (1) describes total FRE emission above the background over an extended wavelength range, whereas spaceborne imaging systems typically measure infrared radiation only in discrete wavelength regions. To tackle this limitation, a relationship must be derived between the individual spectral measurements available from infrared spectro-radiometers and the total amount of energy emitted by the fire over all wavelengths.

One approach is to adopt the Bi-spectral method of Dozier (1981), whereby two measurements of emitted infrared spectral radiance made at well-separated wavelength intervals are used to calculate the effective temperature (T_{EF}) and subpixel area (A_{EF}) of the 'effective emitter' that would reproduce the signal observed in the two spectral regions. Whilst a single temperature and subpixel area clearly does not precisely match the multithermal component structure of the actual fire, with the simplifying assumption that $n = 1$ such retrievals can be used to estimate FRE via an adaptation of Eq. (1). Giglio and Kendall (2001) provide a recent review of the Bi-spectral method and its application to satellite sensor imagery, where it is seen to be subject to large errors if careful consideration of the accuracy of the interchannel registration and background temperature characterisation is not carried out (Langaas, 1995). Nevertheless, the method has been used extensively to calculate the T_{EF} and A_{EF} of remotely sensed fires for over a decade, most commonly from AVHRR and GOES (Prins, Feltz, Menzel, & Ward, 1998; Robinson, 1991), and the BIRD HSRS sensor has been designed to allow accurate use of the technique. The use of the Bi-spectral method in the derivation of FRE is, however, relatively new.

An alternative method for the remote determination of FRE was proposed by Kaufman et al. (1996), based on semi-empirical relationships between FRE and infrared spectral radiances recorded by the MODIS Airborne Simulator. Kaufman, Kleidman, et al. (1998) went onto develop relationships between FRE and the brightness temperatures recorded in the 4 μm channel (band 21) of the EOS MODIS spaceborne instrument. This MODIS method is now used to determine FRE within the MODIS 'fire products' that are being developed to facilitate studies of atmospheric and surface change due to biomass burning and other related factors (Kaufman & Justice, 1998; Kaufman, Justice, et al., 1998; Justice et al., 2002).

Here, we derive a third method to estimate FRE directly from the MIR spectral radiances recorded by the BIRD-HSRS instrument. This method, which we term the MIR radiance method, can also be applied to data from the MODIS sensor or any other sensor possessing a suitably calibrated and non-saturating MIR spectral channel. As with the MODIS method, since the MIR radiance method uses single wavelength observations only it is not subject to the potential errors caused by interchannel spatial misregistration.

3.2. FRE derivation via MIR radiances

The spectral radiance $L(\lambda)$ emitted by a blackbody at wavelength λ is given by the Planck function (Eq. (2)), which can be approximated over a particular temperature range by the simple power law shown as Eq. (3) (Wooster & Rothery, 1997):

$$L(\lambda, T) = \frac{C_1}{\lambda^5\left(\exp\left(\frac{C_2}{\lambda T}\right) - 1\right)} \quad (2)$$

$$L(\lambda) = aT^b \quad (3)$$

where λ is wavelength (m), T is temperature (K), L is spectral radiance W m^{-2} sr^{-1} m^{-1}, C_1 and C_2 are constants (1.19×10^{-16} W m^2 sr^{-1} and 1.44×10^{-2} mK, respectively), and a and b are empirically derived constants, dependent upon both wavelength and temperature range used.

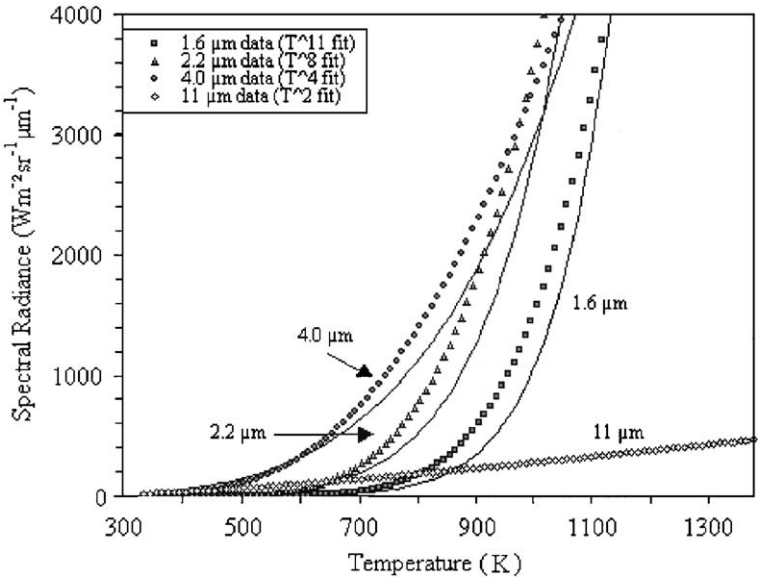

Fig. 2. Planck function (Eq. (2)) relationship between blackbody temperature and emitted spectral radiance at a single wavelength (indicated by the symbols) and Eq. (3) approximation to this (indicated by the solid lines). Relationships are shown for four infrared wavelengths common on satellite-based imaging systems.

Fig. 2 shows the fit between Eqs. (2) and (3) for four infrared wavelengths present on imaging spectro-radiometers such as MODIS, over a temperature range encompassing the majority of vegetation fire activity. What is noticeable is that at wavelengths in the MIR terrestrial atmospheric window (i.e., around 4 μm) the relationship between spectral radiance and emitting temperature approaches that of Stefan's Law, i.e., it is proportional to the fourth power of the emitter temperature. Thus, for the temperature range over which the assumption is valid, the ratio of the total power emitted over all wavelengths (FRE_{TRUE}) to the power emitted at 4 μm (L_{MIR}) is approximately constant. Fig. 3 demonstrates this is true in a temperature range appropriate to most wildfires (~ 600–1500 K) but that the value of the ratio rises sharply at lower temperatures, indicating breakdown of the $L_{MIR} = aT^4$ relationship below a ~ 600 K threshold.

Within the appropriate temperature range, use of the T^4 relationship within an expansion of Eq. (3) to represent a

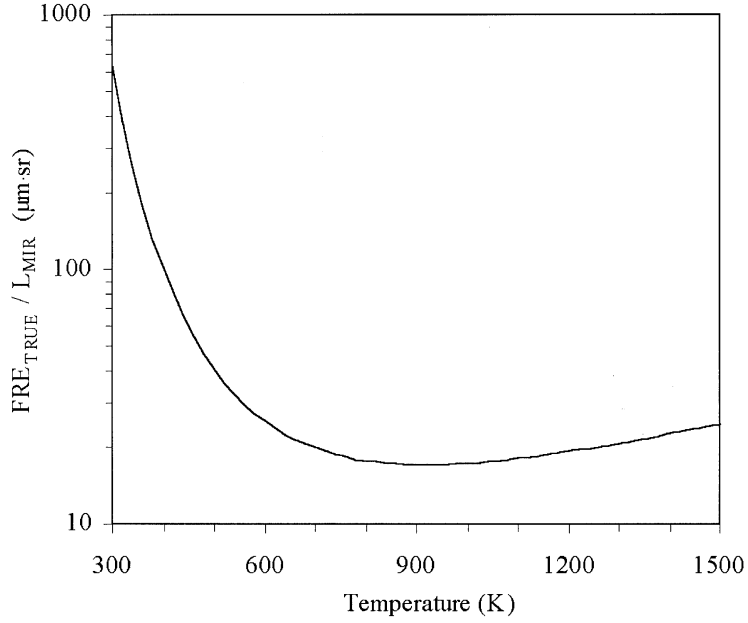

Fig. 3. Ratio of true FRE emitted from a unit area surface to its middle infrared spectral radiance at 4 μm, as a function of surface temperature. In the range 600–1500 K, the ratio has a value 19.68 μm·sr ± 30%.

fire 'hotspot' pixel containing n subpixel thermal components provides Eq. (4):

$$L_{\mathrm{MIR,h}} = a\varepsilon_{\mathrm{MIR}} \sum_{i=1}^{n} A_n T_n^4 \quad (4)$$

where $L_{\mathrm{MIR,h}}$ and $\varepsilon_{\mathrm{MIR}}$ is the hot 'fire' pixel spectral radiance and surface spectral emissivity in the appropriate MIR spectral band and the constant a (W m^{-4} sr^{-1} μm^{-1} K^{-4}) is determined from empirical best-fit relationships such as those shown in Fig. 2. The value appropriate to MODIS band 21 is $a = 3.0 \times 10^{-9}$, whilst that for the HSRS MIR band is 3.3×10^{-9}.

Combining Eqs. (1) and (4) provides Eq. (5), which relates FRE to the MIR spectral radiance of the hot pixel:

$$\mathrm{FRE}_{\mathrm{MIR}} = \frac{A_{\mathrm{sampl}}\sigma\varepsilon}{a\varepsilon_{\mathrm{MIR}}} L_{\mathrm{MIR,h}} \quad (5)$$

Since $L_{\mathrm{MIR,h}}$ represents the MIR radiance from the fire only, when analysing real remotely sensed data this should be calculated by subtracting the background MIR radiance $L_{\mathrm{MIR,bg}}$ (estimated from neighbouring non-fire 'ambient' pixels) from that of the fire pixel. Furthermore, Langaas (1995) suggests fires can be assumed to radiate as grey-bodies (i.e., $\varepsilon = \varepsilon_{\mathrm{MIR}}$), an assumption that can be updated if more accurate flame emissivity data become available. Then, setting A_{sampl} equal 1.0×10^6 m^2 for MODIS, and 3.42×10^4 m^2 for HSRS provides the algorithm for the MIR radiance method of FRE derivation applied to individual HSRS or MODIS pixels:

$$\text{BIRD:}\quad \mathrm{FRE}_{\mathrm{MIR}} = 5.93 \times 10^5 (L_{\mathrm{MIR}} - L_{\mathrm{MIR,bg}}) \quad (6a)$$

$$\text{MODIS:}\quad \mathrm{FRE}_{\mathrm{MIR}} = 1.89 \times 10^7 (L_{\mathrm{MIR}} - L_{\mathrm{MIR,bg}}) \quad (6b)$$

Where all radiances are expressed in units of W m^{-2} sr^{-1} μm^{-1} and FRE in units of J s^{-1} or Watts.

It should be reiterated that Eqs. (6a) and (6b) are based on the approximation $L_{\mathrm{MIR}} = aT^4$ introduced previously, and will therefore fail outside of the ~600–1500 K temperature range where that approximation holds. Fig. 4 demonstrates the validity of the assumption that the relationship between FRE and MIR spectral radiance is independent of target temperature over a range appropriate to most wildfire activity. This figure graphs the various combinations of subpixel hotspot temperature (T) and fractional area (A) that can potentially give rise to a particular MIR signal (in this case 57.6 W m^2 sr^{-1} μm^{-1}) and indicates the FRE value that results from use of these temperature and fractional area combinations in Eq. (1). Below ~500 K, the relationship between FRE and MIR spectral radiance is, in fact, strongly dependent on target temperature and so the FRE estimate is highly sensitive to assumed T. However, above ~600 K, the relationship between FRE and MIR spectral radiance is relatively independent of target temperature and the retrieved FRE shows only small sensitivity to it. Therefore, because vegetation fires are generally hotter than this,

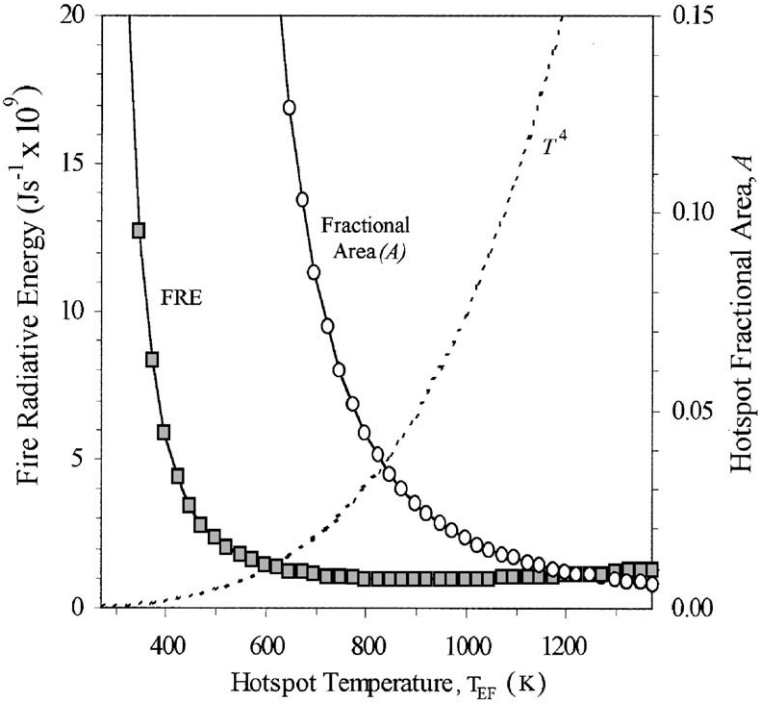

Fig. 4. The range of hotspot pixel fraction and fire radiative energy solutions, calculated using Eqs. (1) and (4) for a MIR wavelength of 4 μm and with assumed hotspot temperatures in the range 0–1100 °C. $L_{\mathrm{MIR,h}}$ was set to 57.6 W m^{-2} sr^{-1} μm^{-1}, equivalent to a hotspot of effective temperature 873 K (600 °C) filling 0.03 of a pixel—this is an equivalent pixel integrated brightness temperature of 473 K, which would not saturate the HSRS sensor but which would saturate MODIS (having a saturation temperature of ~450 K). A Stefan's Law T^4 curve is superimposed.

Eqs. (6a) and (6b) should hold for analysis of real wildfires provided the radiance observations are made in a suitable MIR spectral band. There does, however, remain the issue of 'cooling' ground over which the fire has recently passed and which may therefore be emitting significant amounts of MIR electromagnetic radiation but which will likely be at a temperature below 600 K. This 'cooling ground' may therefore contribute to the MIR radiance signal attributed to fire, but the FRE contribution from this 'cooling ground' component may not be accurately estimated using the MIR radiance method since its temperature is outside of the domain of applicability. This issue will be discussed further during model evaluation (Section 4).

To determine the best wavelength range to make the FRE observations, and to investigate the usefulness of the wider infrared spectral range potentially measurable from low Earth orbit, the spectral radiance emitted from a dual thermal-component fire at wavelengths between 1.5 and 13 μm was modelled via the simple area weighted Planck functions (Eq. (2)) shown in Dozier (1981). These values were compared to that of FRE_{TRUE}, calculated via Eq. (1). The results, shown in Fig. 5, indicate that 98% of the variance in fire radiative energy is explained by variations in the emitted infrared spectral radiance at 4 μm, but that the strength of this relationship decreases rapidly outside of the 3–5 μm spectral region. Thus, sensors such as the HSRS and MODIS, with spectral bands encompassing this MIR region and which are capable of making unsaturated measurements over high intensity targets, are optimum for the remote determination of FRE.

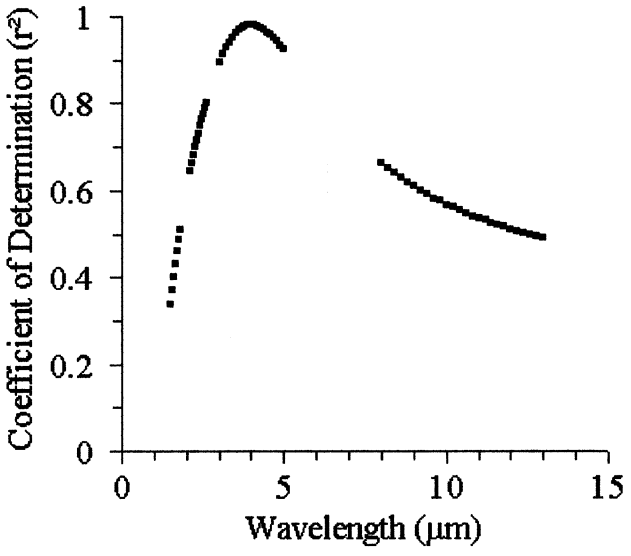

Fig. 5. Coefficient of determination (r^2) between the thermal emission at individual wavelengths located in terrestrial atmospheric windows (1.5–13 μm) and the fire radiative energy emitted over all wavelengths for a dual thermal component fire. Calculation is based on 2000 model simulations, each containing a random temperature component within the flaming (950–1300 K) and cooling–smouldering (350–700 K) range, with each component taking up random proportions of the pixel.

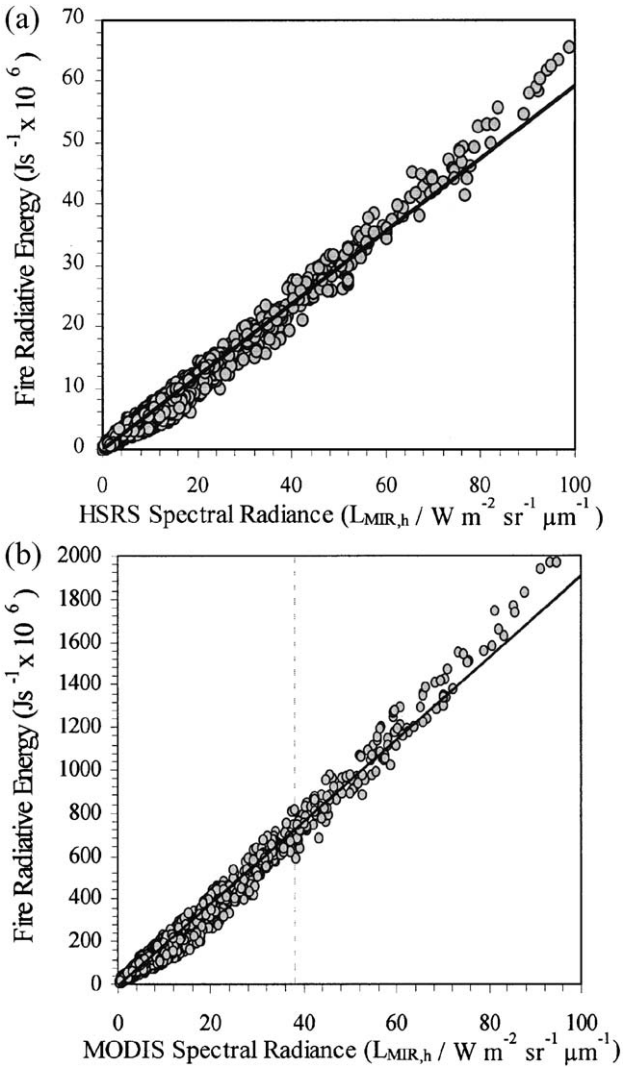

Fig. 6. Relationship between the fire radiative energy emitted over all wavelengths and the composite-fire spectral radiance recorded in (a) the HSRS and (b) the MODIS MIR spectral channels. Data are from 2000 model simulations each containing five random flaming (1000–1300 K) and cooling–smouldering (350–700 K) components of random size, superimposed on a random ambient temperature background (283–303 K). To give pixel integrated brightness temperatures broadly corresponding to those observed in real HSRS and MODIS imagery, for the HSRS simulation, the maximum size of each flaming component was 0.01 pixel and of each cooling–smouldering component was 0.1 pixel, with the values for the larger MODIS pixels a factor of 10 smaller due to its larger pixel area. Eqs. (6a) and (6b) relationships for estimating FRE from HSRS and MODIS MIR channel data respectively are overlain and are seen to be in excellent agreement with the modeled data. Vertical dashed line in (b) indicates the MODIS sensor saturation limit.

3.3. Theoretical testing of FRE derived via MIR radiances

To provide a first test of the capability of Eqs. (6a) and (6b) to retrieving FRE directly from MIR spectral radiances, we conducted simulation modelling of the radiative emission from 2000 subpixel fire scenarios (having cooling, smouldering, and flaming components). This approach

is very similar to that carried out by Kaufman, Justice, et al. (1998) to derive the MODIS method of FRE estimation, but here we are using it to test the accuracy of the MIR radiance method rather than to derive the actual algorithm coefficients. Thermal emittance from the modelled fires was calculated as area-weighted Planck functions (Eq. (2)) incorporating five random hot and five random smouldering-to-cooling components, superimposed on an ambient temperature background. The MIR spectral radiance of the fire ($L_{MIR,h}$) was determined via the radiance difference between the simulated fire pixel (L_{MIR}) and neighbouring ambient-temperature pixels ($L_{MIR,bg}$) (Wooster & Rothery, 1997). In real data, $L_{MIR,h}$ could also be determined via the signal recorded at longer wavelengths deemed to be unresponsive to the subpixel features (Wooster, 2001). FRE_{TRUE} was calculated via Eq. (1) and Fig. 6 indicates that for both sensors the relationship between $L_{MIR,h}$ and FRE_{TRUE} is in excellent agreement with the physically derived Eqs. (6a) and (6b) (BIRD: $r^2 = 0.98$, $n = 2000$, RMSD = 1.2×10^6 J s^{-1}; MODIS: $r^2 = 0.98$, $n = 2000$, RMSD = 65×10^6 J s^{-1}).

4. Simulation-based intercomparison of FRE derivation methods applicable to BIRD

Errors of sensor calibration, atmospheric correction, and assumed fire emissivity will each impact the accuracy of the three FRE estimation methods discussed in this paper when applied to real imagery of active fires. However, by first applying the methods to simulated data derived from models of fire thermal emission, the effects of these perturbations can be removed and the underlying accuracy of the methods better assessed. Two models were used to analyse the performance of the FRE-derivation methods, (i) a homogeneous fire model and (ii) a non-homogeneous fire model.

The homogeneous fire model simulates a hot pixel as a mixture of a homogeneous fire (characterised by a single temperature and subpixel area) and a constant background. Though this model is rather far from reality, it is useful to investigate fire temperature effects on energy release estimation, as well as being the basis for the Bi-spectral method (Dozier, 1981).

The non-homogeneous fire model is closer to reality and simulates a hot pixel as a mixture of three higher temperature components (flaming fire, smouldering fire, and cooling ground) and the ambient background. Each has a gaussian temperature distribution with the parameters shown in Table 2 and the fractional area of each component can vary from 0 to 1.0, under the condition that the MIR radiant temperature of the mixture should not be less than 320 K. This condition excludes pixels dominated by the background and corresponds to the typical MIR threshold temperature for accurate hotspot detection via fire detection algorithms (Zhukov & Oertel, 2001). It should be noted that prior work (Wooster, 2002) that explored the correlation between biomass combusted and fire radiative energy release during the combustion process assumed only two (flaming and smouldering) components. This was appropriate for the ground-based observation of small-scale experimental fires, but as previously mentioned moderate resolution pixel-based views of wildfires advancing through the landscape will most likely also contain areas of 'cooling ground' that have recently been affected by the fire, in addition to the active fire itself and a substantial area of background. We therefore include 'cooling' and 'background' components within the non-homogenous fire model to test the response of the FRE derivation methods to variations in these additional categories. In total, the scenarios tested with the non-homogenous fire model covered 23662 different combinations of flaming, smouldering, cooling, and background.

4.1. Bi-spectral method

The Bi-spectral method of Dozier (1981) has been used extensively to calculate the effective temperature T_{EF} and area A_{EF} of remotely sensed fires (e.g., Giglio & Kendall, 2001; Prins et al., 1998), which can then be used to estimate FRE via Eq. (1), assuming $n = 1$. In order to conform to the

Table 2
The components of the non-homogeneous fire model

Component	Mean temperature (K)	Standard deviation of temperature (K)	FRE per unit area of component (J s^{-1} m^{-2})			
			True value	Bi-spectral method	MODIS-B method	MIR radiance method
Flaming	1000	100	5.97×10^4	5.87×10^4	2.85×10^5	6.36×10^4
Smouldering	600	100	8.06×10^3	8.06×10^3	6.68×10^3	6.30×10^3
Cooling	350	25	$4.17 \times x10^2$	4.16×10^2	5.26×10^1	5.39×10^1
Background	300	10	–	–	–	–

Each component has a gaussian temperature distribution characterised by the mean and standard deviation shown. The true fire radiative energy for each component calculated using Eq. (1) is also shown, along with FRE calculated via each of the three remote sensing methods discussed herein. All FRE values are shown as the value above that of the background and are here expressed per unit area so as to indicate their potential relative contribution to the FRE of real wildfires (prior to consideration of their respective areas).

other two FRE derivation methods considered here, we define FRE_{BS} relative to the background signal:

$$FRE_{BS} = \sigma(T_{EF}^4 - T_{bg}^4)A_{EF} \quad (7)$$

where T_{bg} is the background temperature estimated from the TIR channel. Accounting for the background is most necessary when considering smouldering fires. For example, the background energy release is 6% of the total fire energy release at a temperature of 600 K.

To mitigate the potentially significant errors introduced to the Bi-spectral method by the imprecise co-registration between the two spectral channels used, when analysing BIRD HSRS data, the Bi-spectral method is applied to contiguous clusters of hotspot pixels detected by the HSRS rather than to each individual pixel (Zhukov & Oertel, 2001). This approach avoids the potentially large retrieval errors in T_{EF} and A_{EF} due to:

- interchannel MIR/TIR geometric co-registration errors;
- point-spread function (PSF) differences between the MIR and TIR channels.

As previously discussed, the values of discrete fire temperature (T_{EF}) and area (A_{EF}) returned by the Bi-spectral method are a clear simplification in that real fires will have many thermal components. To analyse the effect of fire non-homogeneity on the accuracy of FRE_{BS}, we used the non-homogeneous fire model. The values of T_{EF} and A_{EF} were calculated via the Bi-spectral method for each of 23662 combinations of the four thermal components of this model and total FRE_{BS} estimated from Eq. (7). FRE_{BS} was then compared with FRE_{TRUE}, calculated from the summation of the energy release over all the fire thermal components via Eq. (1). Results are shown in Fig. 7 and indicate that the Bi-spectral method leads to an underestimation of FRE for non-homogeneous fires (i.e., $FRE_{BS}/FRE_{TRUE} < 1$). In the presence of only one type of fire activity (i.e., flaming, smouldering, or cooling), but where activity within that type is non-homogeneous, error in FRE determination remains below 2%. The largest deviations occur when the mixture contains all four thermal components, with the background and the cooling fire scars dominating the mixture and where the fractional area of the hotter flaming and smouldering components does not exceed ~1% of the pixel. Even in this highly non-homogenous situation, the error in FRE determination via the Bi-spectral method is less than 11% (i.e., in Fig. 7 $FRE_{BS}/FRE_{TRUE} > 0.89$). Thus, though assumption of a thermally homogeneous fire is at best only a rough approximation to reality, it accounts reasonably well for the temperature distribution effect during the determination of FRE.

A disadvantage of the Bi-spectral method when compared to the alternatives is, however, that it relies on an estimate of the TIR background signal. This can be problematic since the background contribution to the pixel-averaged TIR radiance of the fire pixels is likely to be significantly larger than the fire contribution, and thus inaccuracy in the TIR background radiance estimation can introduce significant errors into the Bi-spectral retrievals of T_{EF} and A_{EF}. As explained by Dozier (1981) and Kaufman et al. (1996), the background signal is typically estimated

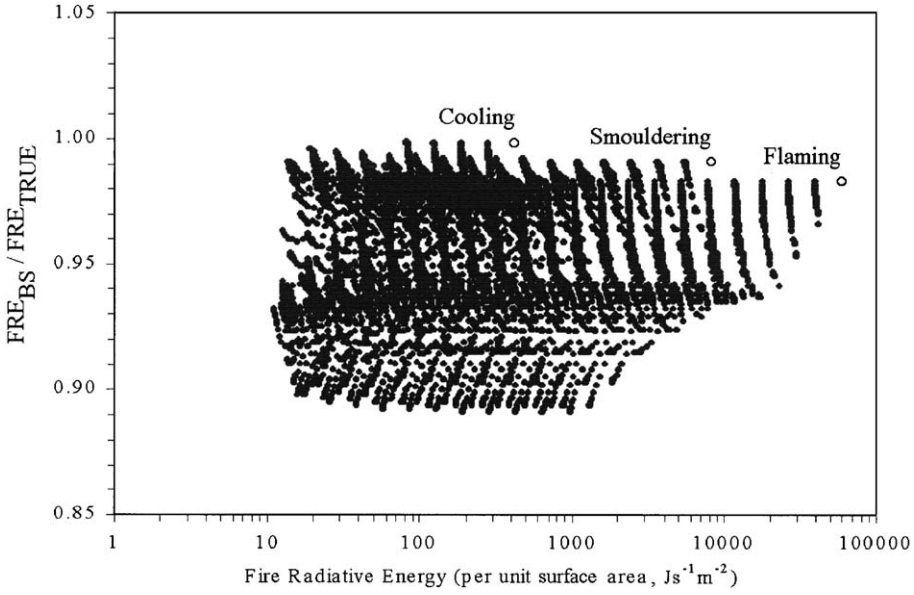

Fig. 7. Ratio of FRE estimated via the Bi-spectral method to the true FRE for the non-homogeneous fire model. Open circles represent the separate flaming, smouldering and cooling components covering 100% of area (with the gaussian temperature distributions shown in Table 2), whereas the dots represent mixtures of these and the ambient temperature background. Note *y*-axis scale compared to that of Figs. 10 and 12 and that actual FRE (*x*-axis) is here expressed per unit area of the surface, only some of which will be covered by fire.

using neighbouring non-hotspot pixels, but errors occur if these pixels do not perfectly characterize the actual background of the hotpot pixels of interest. The sensitivity of FRE_{BS} to errors in the TIR background temperature is illustrated in Fig. 8. Taking q_{EF} as the mean fire proportion in the cluster of pixels ($q_{EF}=A_{EF}/n_{cl}$; where n_{cl} is the number of cluster pixels) then in the case of smaller fires ($q_{EF} \leq 0.001$) if the background temperature estimate possesses an error of ± 5 K the retrieval errors may reach hundreds of Kelvin in T_{EF} and orders of magnitude in q_{EF}. Though such errors in T_{EF} and q_{EF} partly compensate each other during calculation of FRE via Eq. (7), this ± 5 K uncertainty in the TIR background temperature estimate results in potentially large FRE errors for small fires. Fortunately, however, analysing hot pixel clusters rather than individual single pixels can reduce the occurrence of such large errors. Nevertheless, the effect far outweighs that introduced by any uncertainty in MIR background characterization, which generally results in negligible errors in FRE since the fire contribution to the pixel-averaged MIR radiance is typically far stronger than that of the background. This is fortunate since characterization of the MIR background is used in all three approaches to FRE estimation.

Our findings with regard to the Bi-spectral method mirror those of Giglio and Kendall (2001) who studied the sensitivity of the technique to the various error sources present in moderate-to-low spatial resolution instruments such as MODIS and GOES. They suggested that a reasonable limit for reliable application of the Bi-spectral method is $q_{EF}>0.005$, meaning that only larger fires can have their size and temperature retrieved with reasonable uncertainty via this method. However, since the BIRD-HSRS pixel area is around seven times smaller than that of MODIS at nadir, many more fires meet this size criterion with BIRD than with MODIS.

4.2. The MODIS method adapted to BIRD (MODIS-B)

The MODIS method of FRE derivation relates the energy release of the fire pixel to the brightness temperature recorded in the MODIS MIR channel (Justice et al., 2002; Kaufman, Justice, et al., 1998; Kaufman, Kleidman, et al., 1998). Kaufman and Justice (1998) propose that atmospheric correction be applied to the 4 μm data prior to FRE derivation, but at present the MODIS fire products use top-of-atmosphere brightness temperatures only. The MODIS method can be simply adapted to provide FRE from the hot clusters identified in the BIRD images by simply summing the energy release of the single pixels making up the cluster. This 'MODIS method adapted to BIRD' ($FRE_{MODIS-B}$) is given by:

$$FRE_{MODIS-B} = k_{MODIS-B} \cdot 4.34 \cdot 10^{-19} A_{sampl} \sum (T_{MIR}^8 - T_{MIR,bg}^8) \quad [J\ s^{-1}] \qquad (8)$$

where T_{MIR} and $T_{MIR,bg}$ are the MIR brightness temperatures of the fire pixel and of the background (K). The constant $4.34 \cdot 10^{-19}$ was obtained by Kaufman, Justice, et al. (1998) and Kaufman, Kleidman, et al. (1998) when deriving the original MODIS method algorithm using modelling very similar to that used to produce the data of Fig. 6.

We have introduced a constant $k_{MODIS-B}$ into Eq. (8) to account for the difference between the spectral range of the BIRD-HSRS MIR channel (3.4–4.2 μm) and that of the much narrower MODIS MIR channel (3.929–3.989 μm) for which the algorithm was originally derived. The value of this constant was derived via the comparison of MODIS and BIRD data discussed in Section 5.2.

The principal advantage of the MODIS-B method as applied to BIRD data is its better stability during analysis of FRE from smaller fires when compared to the Bi-spectral method. Its principal disadvantage is that, unlike the Bi-spectral method, variations in fire temperature are not explicitly accounted for. For the homogeneous fire model, Fig. 9 illustrates the effect of varying fire temperature via the ratio of $FRE_{MODIS-B}$ to FRE_{TRUE}. For fires hotter than about 600 K but smaller than 0.1 of a pixel the MODIS-B method provides FRE to an accuracy of a few tens of percent. However, the error increases significantly for larger fires (q_{EF} approaching 1.0), as well as for smouldering or cooling activity with temperatures below 600 K. The likelihood of fires occupying the majority of a pixel is clearly greater with BIRD than with MODIS, due to the smaller HSRS pixel size. In fact, when the MODIS FRE algorithm was derived empirically by Kaufman, Justice, et al. (1998) and Kaufman, Kleidman, et al. (1998), the MODIS method coefficients were optimised for retrieval of fire radiative energy from pixels with a maximum MIR brightness temperature around 450 K. This was eminently sensible since this is the specified saturation temperature of MODIS band 21 and, given the 1 km^2 nadir spatial resolution of the MODIS MIR channel, fires large enough raise the MODIS MIR signal to this level were expected only very rarely. However, given the smaller BIRD pixel size the likelihood of the HSRS MIR channel exceeding a 450 K brightness, temperature is significantly increased over MODIS and, for the largest and most intense fires observed by BIRD, the possibility exists that a pixel will comprise mainly flaming combustion ($\sim$ 1000 K). The BIRD HSRS sensor was designed to handle this eventuality and so we must examine the performance of the MODIS-B method in this regime, even though the original MODIS FRE algorithm was not explicitly designed to cope with such situations.

Fig. 10 confirms the above findings for the non-homogeneous fire model. Specifically, the MODIS-B method provides reasonable accuracy in FRE when smouldering fires dominate the mixture, it under-estimates FRE by a factor of up to 8 when cooling ground dominates, and it overestimates FRE by up to a factor of 5 when

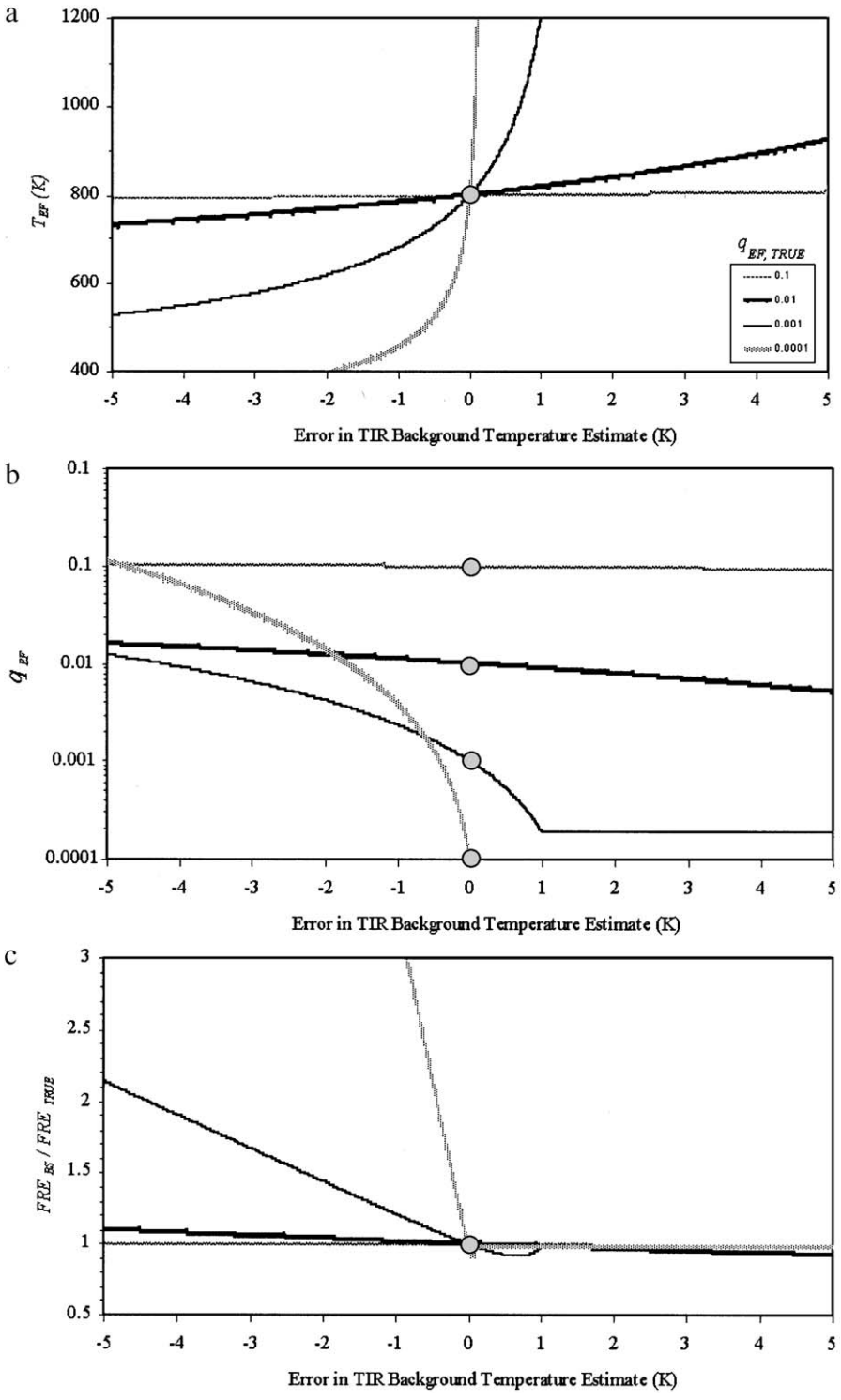

Fig. 8. Effect of errors in the TIR background temperature assumed in the Bi-spectral method on (a) effective fire temperature T_{EF}, (b) mean fire proportion in the cluster pixels $q_{EF} = A_{EF}/n_{cl}$, where n_{cl} is the number of cluster pixels, and (c) FRE release. In this example, the actual background temperature = 300 K, the actual fire effective temperature $T_{EF} = 800$ K and the curves provide the retrieval values of each parameter for actual fire effective proportion $q_{EF,TRUE} = 0.1$, 0.01, 0.001, and 0.0001. The circles correspond to the true fire parameters in each case. During calculations, if the effective fire temperature exceeds 1200 K, it was reset to 1200 K and the fractional area re-calculated for this temperature using the MIR radiance. For comparison, calculated q_{EF} for detected hot clusters in the BIRD images of the Sydney fires shown in Fig. 15 lie between 1×10^{-4} and 1×10^{-2}.

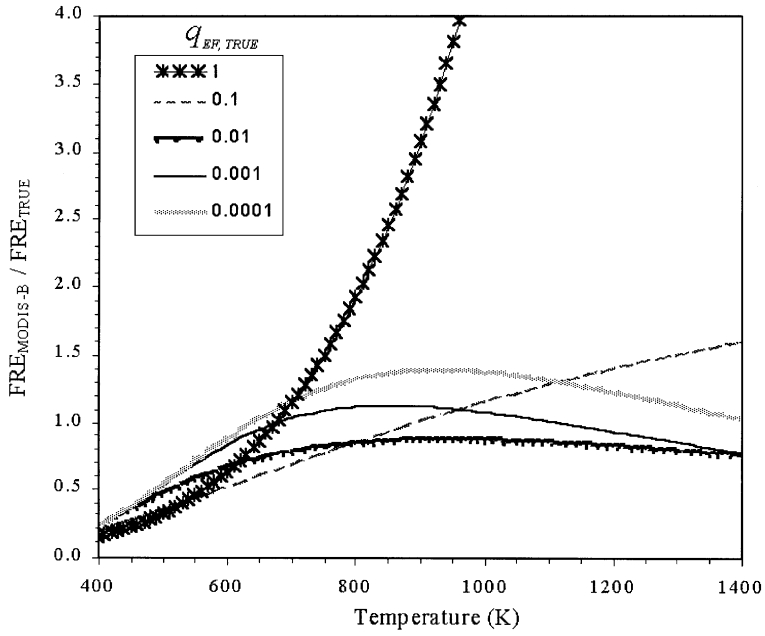

Fig. 9. Ratio of FRE estimated via the MODIS-B method to the true FRE as a function of the fire temperature and proportion in a pixel ($q_{EF,TRUE}$) for the homogeneous fire model.

flaming fires occupy the entire pixel. Fig. 11 shows the same data but with the accuracy of the MODIS-B method of FRE derivation expressed as a function of the effective fire temperature (T_{EF}). The MODIS-B method is seen to be potentially applicable when T_{EF} rises above ~600 K, but there is a tendency to overestimate at high T_{EF}. The most extreme overestimate occurs if flaming combustion fills the entire pixel, in which case FRE is 5× overestimated.

Like the Bi-spectral method, uncertainties in the MIR background characterisation should not significantly impact FRE retrieval accuracy when using the MODIS-B method with BIRD data. For example, if a MIR background temperature of 300 K and an uncertainty of 5 K is

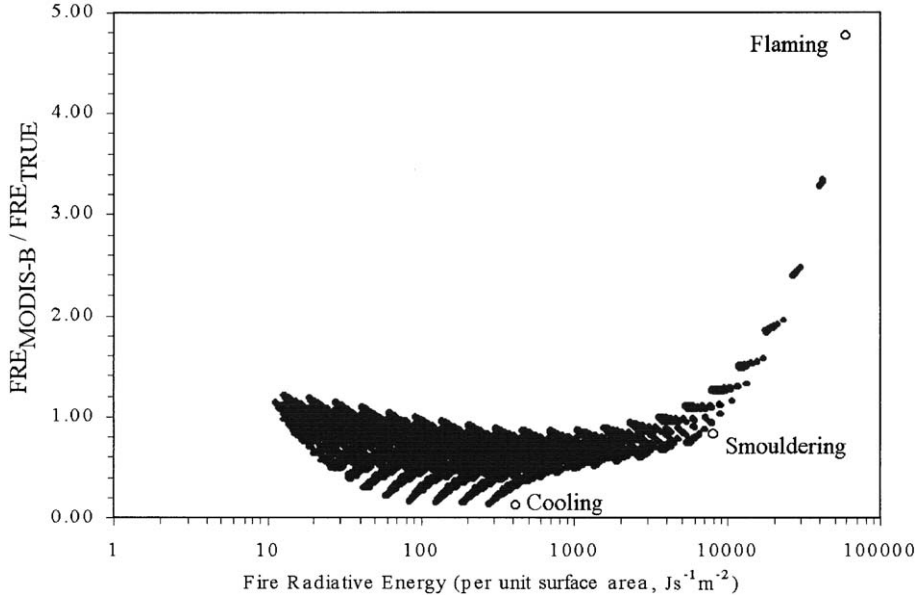

Fig. 10. Ratio of FRE estimated via the MODIS-B method to the true FRE for the non-homogeneous fire model. Open circles represent the separate flaming, smouldering, and cooling components covering 100% of area (with the gaussian temperature distributions shown in Table 2), whereas the dots represent mixtures of these and the ambient temperature background. Note *y*-axis scale compared to that of Figs. 7 and 12 and that actual FRE (*x*-axis) is here expressed per unit area of the surface, only some of which will be covered by fire.

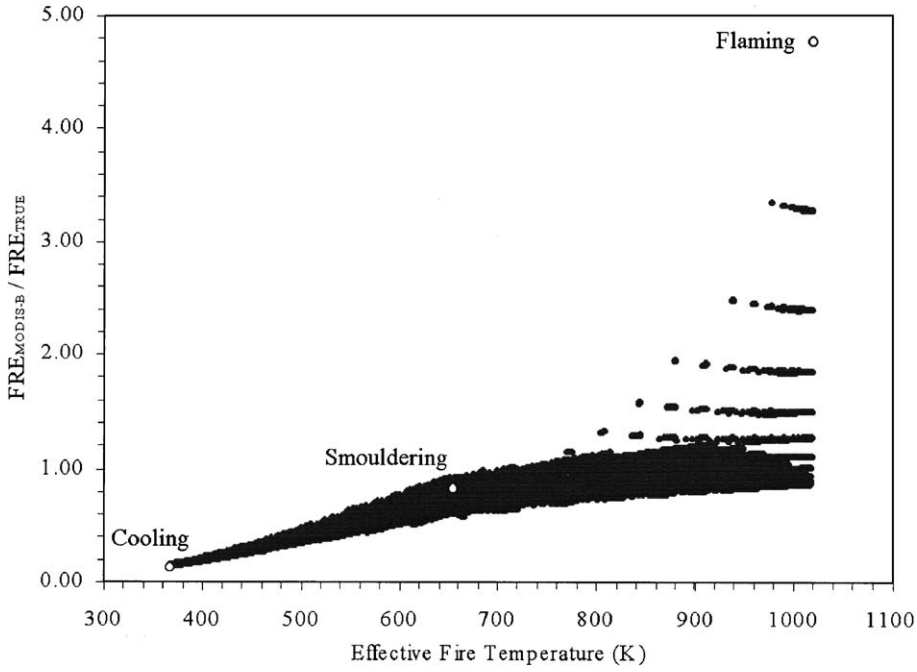

Fig. 11. Errors of the MODIS-B method of FRE retrieval as a function of the effective fire temperature (T_{EF}) for the non-homogeneous fire model. Open circles represent the separate flaming, smouldering, and cooling components, whereas the dots represent mixtures of these and the ambient temperature background. T_{EF} is equivalent to the sub-pixel temperature of the effective hot emitter that would provide the observed radiant signal, as calculated by the Bi-spectral technique. Note *y*-axis scale compared to Fig. 13.

assumed, then the potential error in $FRE_{MODIS\text{-}B}$ estimated via Eq. (8) is only ~ 10% even for fire pixels approaching the limits of detection (i.e., having pixel-integrated MIR temperatures around 320 K). The MODIS-B method is not influenced by any uncertainty in the TIR background characterisation.

4.3. The MIR radiance method

The proposed MIR radiance method for FRE estimation is based on the assumption that total FRE per unit surface area is linearly proportional to the spectral radiance recorded in the MIR waveband, L_{MIR}. The applicability

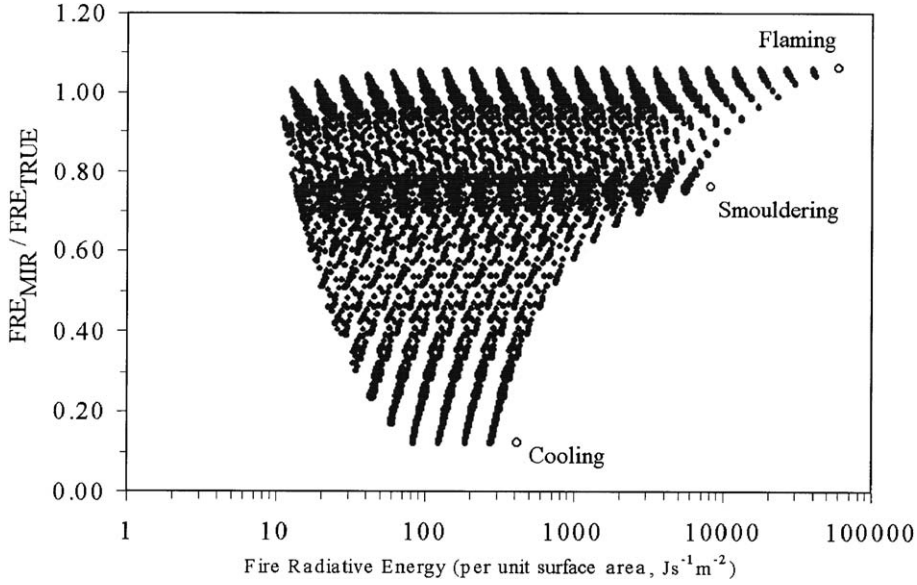

Fig. 12. Ratio of FRE estimated via the MIR radiance method to the true FRE for the non-homogeneous fire model. Open circles represent the separate flaming, smouldering, and cooling components covering 100% of area (with the gaussian temperature distributions shown in Table 2), whereas the dots represent mixtures of these and the ambient temperature background. Note *y*-axis scale compared to that of Figs. 7 and 10 and that actual FRE (*x*-axis) is here expressed per unit area of the surface, only some of which will be covered by fire.

of this assumption was demonstrated in Fig. 3, where as the temperature of the emitter increases from 600 to 1500 K the ratio FRE_{TRUE}/L_{MIR} is seen to vary in a relatively narrow range of 17–25 μm·sr. Only at lower temperatures does the ratio show a strong temperature sensitivity, approaching ~1000 μm·sr at ambient temperatures. The MIR radiance method can be applied for FRE estimation of hot clusters detected by BIRD by applying Eq. (6a) to each detected hot pixel and then summing FRE over all pixels in each cluster, estimating the MIR background radiance $L_{MIR,bg}$ in each case from neighbouring non-fire pixels.

Fig. 12 illustrates the errors of the MIR radiance method for the non-homogeneous fire model. In contrast to the MODIS-B method, the MIR radiance method performs well both for small and large fires in the case when flaming and smouldering components dominate the mixture. However, as with the MODIS-B method, when cooling components dominate the mixture, FRE can be underestimated by a factor of up to 8 due to breakdown of the assumptions at lower temperatures (Fig. 3). Fig. 13 shows the same data but with the accuracy of the MIR radiance method expressed as a function of the effective fire temperature (T_{EF}). The MIR radiance method is seen to be applicable when T_{EF} rises above ~600 K, which is quite usual with BIRD HSRS data. Fire activity within a pixel can include significant low temperature (cooling) components and still meet this criterion, provided they are not dominant such that $T_{EF} < 600$ K. Compared to the MODIS-B method (Fig. 11), the MIR radiance method provides minimal FRE overestimation at high values of T_{EF}, even when flaming combustion fills the pixel. So, when applying the MIR radiance method, if T_{EF} is below 600 K for a particular pixel, then either the Bi-spectral method should be used (where the sensor resolution and background temperature stability allow this) or major underestimation of FRE must be assumed. Again, as with the MODIS-B method, the level of uncertainty in the MIR background temperature is not critical to the accuracy of FRE derivation. If, as before, 320 and 300 K are assumed for the MIR temperatures of the hotspot and background pixels respectively, then an error of 5 K in background temperature estimation results in an FRE error of only ~10%. As with the MODIS-B method, the MIR radiance method is unaffected by any errors in the TIR background characterisation.

5. Data-based intercomparison of FRE derivation methods

5.1. Fire pixel detection

In late December 2001 and January 2002, large-scale bushfires started in a number of national parks surrounding Sydney, Australia (Fig. 14). Daytime temperatures of up to 38 °C, accompanied by winds gusting over 60 km h^{-1}, aided fire development and by 9 January more than 80 individual fires had burned an area estimated at larger than 570,000 ha. BIRD targeted this activity for data acquisition, and largely cloud-free views were obtained on 4, 5, and 9 January 2002 (Fig. 15). Hotspot pixels were detected using

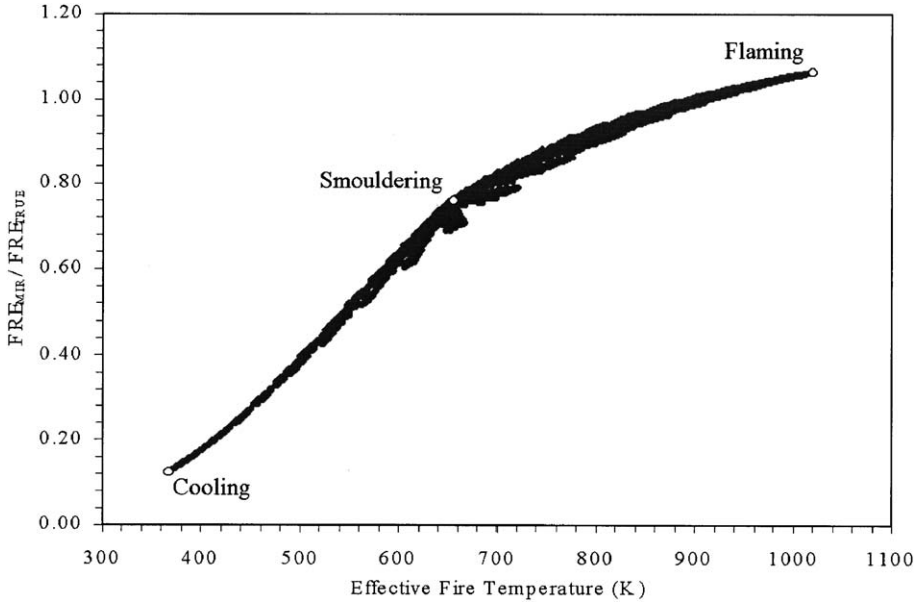

Fig. 13. Errors of the MIR radiance method of FRE retrieval as a function of the effective fire temperature (T_{EF}) for the non-homogeneous fire model. Open circles represent the separate flaming, smouldering, and cooling components, whereas the dots represent mixtures of these and the ambient temperature background. T_{EF} is equivalent to the subpixel temperature of the effective hot emitter that would provide the observed radiant signal, as calculated by the Bi-spectral technique. Note *y*-axis scale compared to Fig. 11.

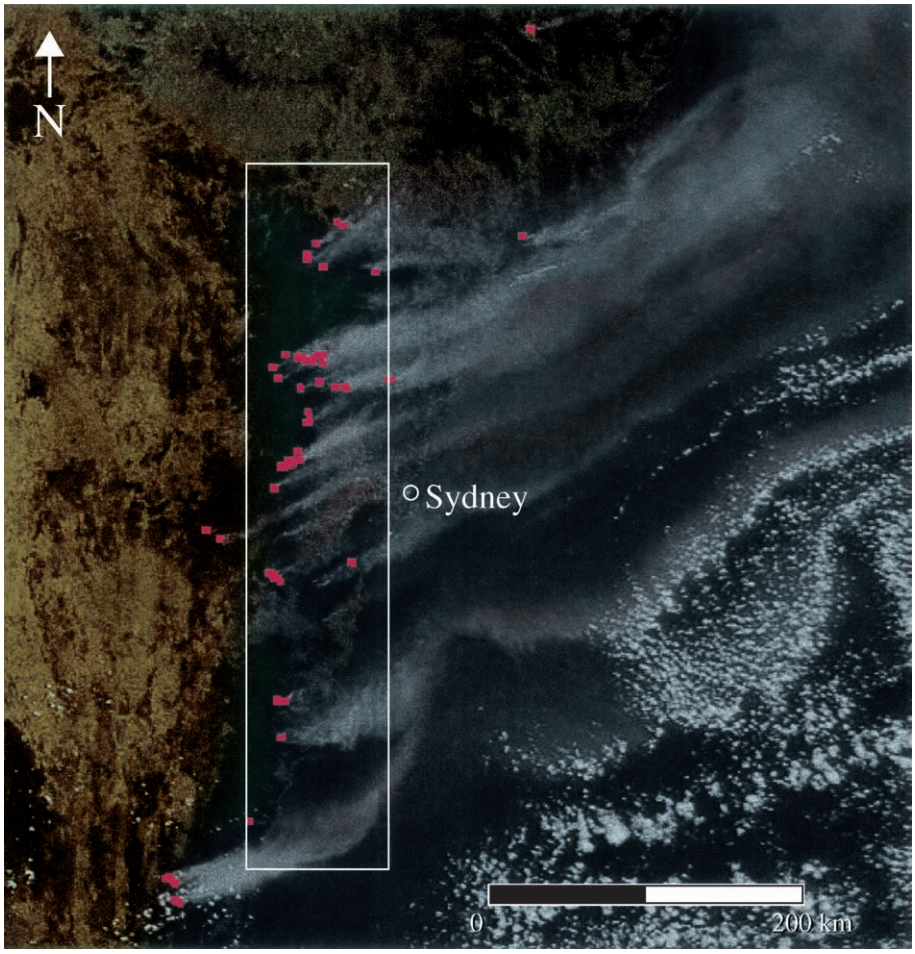

Fig. 14. True-color MODIS subscene of bushfires burning around Sydney, Australia on 3 January 2002. Locations of the most intensely burning fires (shown in red) were detected via thresholding of the MODIS MIR (band 21) data. Smoke from these fires streams away to the northeast. The image was adapted from the NASA Visible Earth database (credit: NASA/Jacques Descloitres, MODIS Land Rapid Response Team, NASA/GSFC). The approximate coverage of the BIRD-HSRS images shown in Fig. 15 is outlined.

the BIRD hotspot detection algorithm of Zhukov and Oertel (2001). This algorithm is based upon a series of multi-spectral tests:

(i) Adaptive MIR thresholding to detect potential hot pixels containing active fires
(ii) Fixed NIR thresholding to reject pixels affected by strong sun glint during daytime observations
(iii) Adaptive MIR/NIR spectral radiance ratio thresholding to reject pixels contaminated by weak sun glint, clouds, and other highly reflective objects during daytime observations
(iv) Adaptive MIR/TIR spectral radiance ratio thresholding to reject warm surfaces heated, for example, by insolation.

The colour coded hotspot pixels of Fig. 15, having MIR brightness temperatures above 330 K, are clearly identifiable as belonging to fire fronts and these, along with a small number of pixels with somewhat lower MIR brightness temperatures, were detected as containing fires by the BIRD hotspot detection algorithm. Having identified the 'fire' pixels, the algorithm then groups neighbouring hotspot pixels into individual 'hot clusters', in this case 544 clusters in the three images, and applies the Bi-spectral method of Dozier (1981) to retrieve the effective fire temperature T_{EF} and area A_{EF} for each cluster. On 4 and 5 January, it can be seen that burning was occurring over extended fire fronts and the data of Table 3 suggests that fire activity to the south of Sydney was somewhat suppressed on 5 January compared to 4 January, though the situation is a little uncertain because of light cloud cover. By 9 January, most of the northern fires were extinguished but widespread burning continued in central and southern areas.

The Sydney fires were imaged by MODIS at 10:22 a.m. local time on 5th January 2002, within 12 min of the BIRD overpass. Fig. 16 shows the MODIS MIR (band 21) subscene corresponding to the BIRD-HSRS MIR image of Fig. 15b, and Fig. 17 shows further enlargements of corresponding parts of these MODIS and BIRD images, and of the corresponding 'fire pixel masks'. The BIRD fire

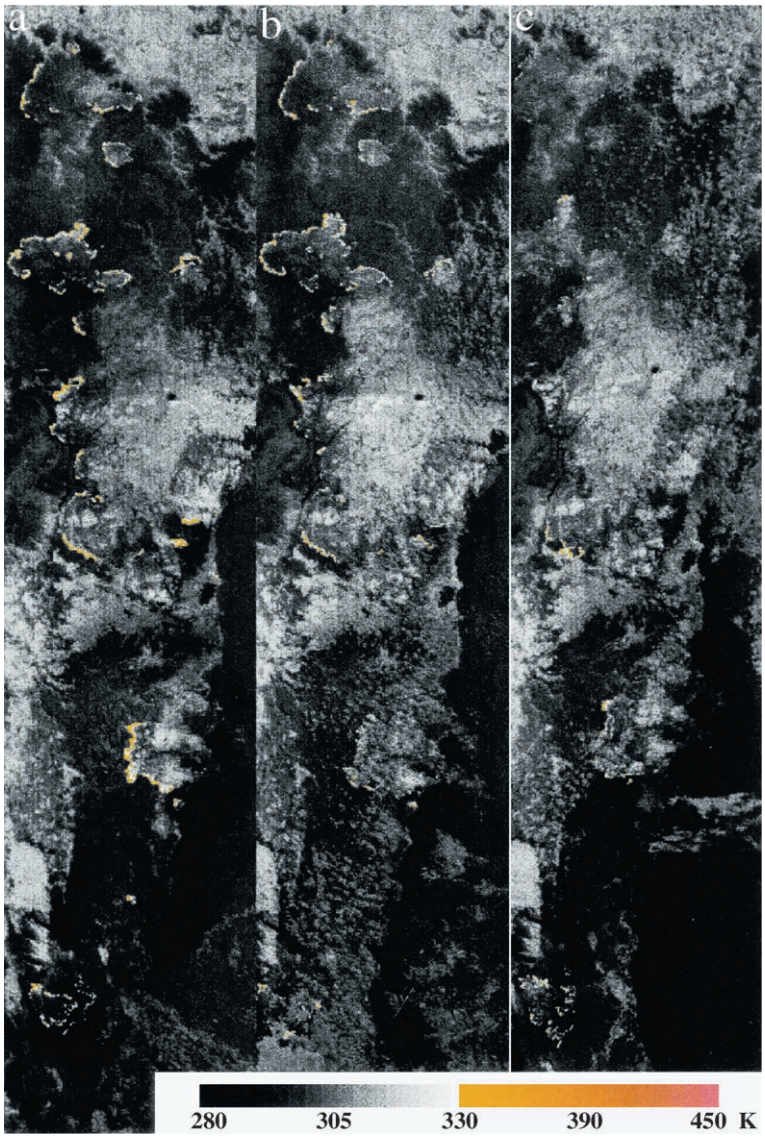

Fig. 15. Three BIRD-HSRS daytime brightness temperature images of the Sydney bushfires obtained in the MIR band (3.4–4.2 μm) a few minutes after 00:00 GMT on (a) 4 January 2002, (b) 5 January 2002, and (c) 9 January 2002. Pixels with MIR brightness temperatures above 330 K are colour-coded. These pixels (along with some of the brightest greyscale pixels having brightness temperatures above 322 K) were those recognised as containing active fires using the BIRD hot-spot detection algorithm of Zhukov and Oertel (2001). North is approximately towards the top of the figure and each scene covers a 400 × 90 km area matching the region outlined in Fig. 12.

mask is that produced via the BIRD hot-spot detection algorithm described above, whilst the MODIS fire mask is that obtained from the MODIS 'MOD 14' fire product that is based on the results of fire detection algorithms described in Kaufman and Justice (1998) and Kaufman, Justice, et al. (1998).

The higher spatial resolution of the HSRS sensor allows recognition of individual fire fronts, whereas only individual hot pixels or small groups of pixels are detected in the MODIS fire product. Comparison of the data shown in Fig. 17 indicates, however, that many more fire pixels can be detected visually in the MODIS MIR band 21 data than are indicated by the MODIS fire product. However, the MIR brightness temperature of most of these unidentified fire pixels does not exceed that of the sparsely vegetated area in the lower right of the larger MODIS subscene shown in Fig. 16, indicating some of the difficulty faced by automated fire detection algorithms. Totally, in the area shown in Fig. 17, the BIRD fire detection algorithm selected 1135 hotspot pixels in the HSRS data (corresponding to a total area of 39 km^2), whereas the MODIS fire detection algorithm selected 19 hotspot pixels in the MODIS data (corresponding to a total area of 25.7 km^2 with the 1.35 km^2 pixel size at this 26° zenith angle (Nishihama et al., 1997)). Whilst it should be remembered that none of these pixels were likely to have been fully filled by fire, many of the BIRD pixels maybe filled by fire to a greater degree because they are 7 × smaller in area than those of MODIS at this scan angle. Thus, it

Table 3
Fire characteristics in the BIRD image swaths shown in Fig. 15

Date	Hot clusters	Hot pixels	Hot pixel area (km^2)	Effective fire area from Bi-spectral method (km^2)	Fire radiative energy release (all clusters) J $s^{-1} \times 10^9$		
					Bi-spectral method	MODIS-B method	MIR radiance method
4 January	221 (124)	4550	155.7	0.18–2.8	15.2 (13.3–20.0)	13.2	14.1
5 January	215 (135)	2208	75.6	0.06–0.94	6.5 (6.0–8.3)	6.1	6.4
9 January	108 (60)	854	29.2	0.02–0.60	2.5 (2.2–3.4)	2.2	2.3

Cluster number in brackets correspond to clusters where FRE retrievals by the Bi-spectral method varied by less than 30% when $\bar{L}_{TIR,bg}$ was varied in the range $\pm \sigma_{TIR,bg}$, where $\bar{L}_{TIR,bg}$ and $\sigma_{TIR,bg}$ are the mean and standard deviation of the TIR radiance of the background pixels surrounding each cluster. FRE calculations based on the three independent methods agree rather well.

seems clear that BIRD detects significantly more fire activity than does MODIS, which can be seen visually by comparing Fig. 17c and d, and this is largely due to the smaller HSRS MIR pixel area. With a fire detection strategy based on MIR brightness, temperature thresholding alone and, with all other factors being equal, the 7× pixel area difference between the two sensors at nadir results in the BIRD HSRS minimum detectable fire area being 7× smaller than that of the nadir MODIS view. Clearly, the BIRD and MODIS fire detection algorithms are more sophisticated than this, and also differ in their detail. Nevertheless, the fact that even a 5 K change in the MIR fire detection brightness temperature threshold changes the minimum detectable fire area by only ~ 20% suggests that it is the higher spatial resolution of BIRD, rather than the specifics of the fire detection algorithm used, that is primarily responsible for its improved performance in identifying hotspot pixels. Nevertheless, it should be recognized that the MODIS fire detection algorithm had to be fully specified before the Terra satellite launch (Kaufman & Justice, 1998; Kaufman, Justice, et al., 1998) and that its sensitivity to small fires can almost certainly be improved

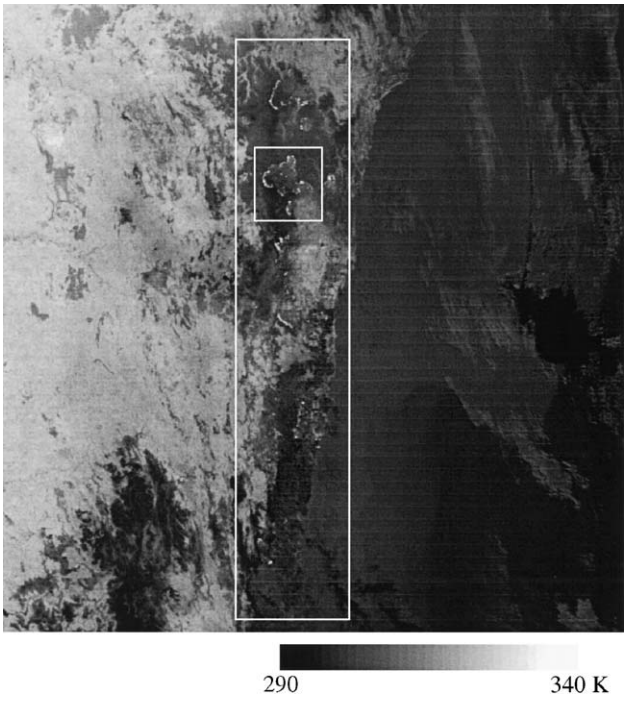

Fig. 16. Daytime brightness temperature image of the Sydney bushfires obtained in MODIS channel 21 (3.929–3.989 μm) at 00:22 GMT on 5 January 2002, 12 min after the corresponding BIRD scene of Fig. 15b. A 500 × 500 km subscene is shown and the areas outlined are that corresponding to that of the BIRD scene of Fig. 15b (large box) and the fire group shown in Fig. 17 (small box). Note the lack of any obvious signal scattering by the fire plumes shown in Fig. 14 since smoke is broadly transparent at this MIR wavelength.

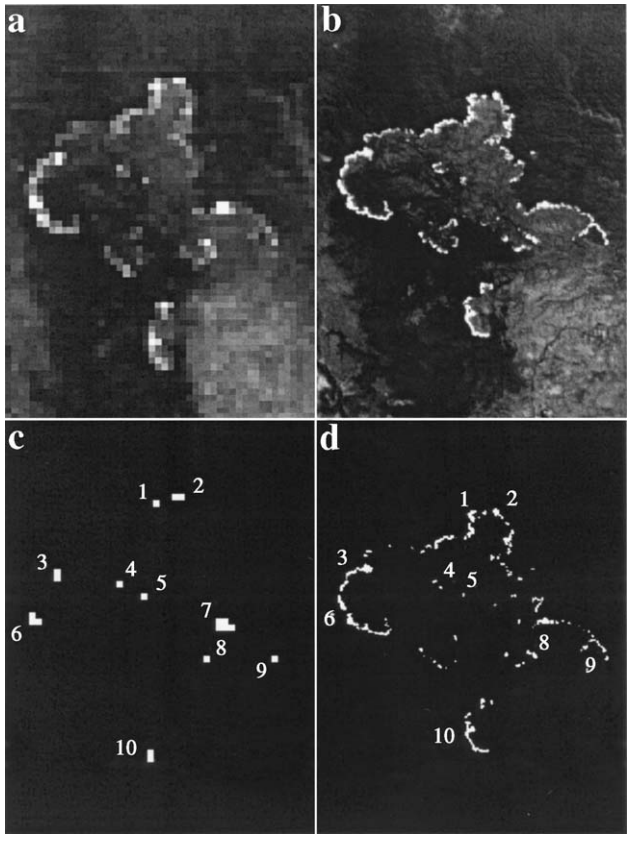

Fig. 17. MODIS and BIRD daytime brightness temperature subscenes, extracted from the 5 January 2002 imagery shown in Figs. 16 and 15b, respectively, along with image masks showing fire pixels identified in the area outlined by the small box in Fig. 16. (a) MODIS band 21 raw data, (b) BIRD MIR band raw data, (c) MODIS fire pixels detected as containing active fires in the MODIS fire product (Kaufman & Justice, 1998), and (d) BIRD pixels detected as containing active fires by the BIRD hot-spot detection algorithm (Zhukov & Oertel, 2001). Ten discrete pixel groups are labelled in the MODIS fire mask. Corresponding 'hot clusters' of neighbouring or near-neighbouring fire pixels are identified in the BIRD fire mask.

now that real MODIS data are available and are being processed to generate fire products for validation by the science community (Justice et al., 2002). The algorithm is therefore undergoing detailed testing and adaptation to further improve its global effectiveness and in particular its sensitivity to smaller fires (Louis Giglio, personal communication), which should in turn improve its ability to determine total FRE.

5.2. FRE derivation from BIRD

For the purpose of the FRE algorithm intercomparison for use with BIRD and for derivation of the factor $k_{\text{MODIS-B}}$ used in Eq. (8), it was advantageous that uncertainty in the Bi-spectral retrievals introduced by potential errors in the TIR background characterisation had minimal effect. Therefore, the 544 hot clusters detected by BIRD and shown in Fig. 15 were first checked for stability of the Bi-spectral retrievals with regard to the TIR background temperature. This was carried out by varying the TIR background radiance around its assumed value $\bar{L}_{\text{TIR,bg}}$ in the range of $\pm\sigma_{\text{TIR,bg}}$, where $\bar{L}_{\text{TIR,bg}}$ and $\sigma_{\text{TIR,bg}}$ are the mean and standard deviation of the TIR radiance of the background pixels surrounding each hot cluster. The requirement for stability was set so that the corresponding variation in FRE_{BS} did not exceed 30%, and this resulted in the removal of 225 clusters from this comparison, these clusters having Bi-spectral retrieval uncertainties exceeding this threshold. Clearly, the Bi-spectral retrieval for an intensely radiating cluster will be stable at a level of TIR background temperature variation that might make that of a weaker radiating cluster unstable. However, it was found that the primary reason for clusters having an unstable Bi-spectral retrieval was that they were located in areas of highly non-homogeneous background (the median TIR background temperature standard deviation for the 'unstable' clusters was 2.6 K compared to that of 1.6 K for the 'stable' clusters) rather than that they were weakly radiating (median FRE of 'unstable' clusters was 13.5×10^6 J s^{-1}, only slightly lower than that of 15×10^6 J s^{-1} for the 'stable' clusters).

The retained 319 'reference' clusters contained 53% of all HSRS detected hotspot pixels. The three FRE derivation methods were then applied to these clusters to intercompare the different methods of FRE retrieval applicable to BIRD HSRS data:

(a) the Bi-spectral method (Dozier, 1981),
(b) the MODIS method adapted to BIRD (so called MODIS-B) (Kaufman, Justice, et al., 1998; Kaufman, Kleidman, et al., 1998), and
(c) the MIR radiance method proposed in the present paper.

In Fig. 18, a strong correlation is evident between results obtained with each of the three FRE derivation methods. From the regression of FRE_{BS} and $\text{FRE}_{\text{MODIS-B}}$ (Fig. 18a), the factor $k_{\text{MODIS-B}}=0.605$ for use in Eq. (8) was derived to allow the adapted MODIS method to provide quantitatively meaningful results when applied to HSRS data. The strong agreement between FRE_{BS}, which inherently accounts for fire temperature effects, and $\text{FRE}_{\text{MODIS-B}}$ and FRE_{MIR}, which do not, indicates that

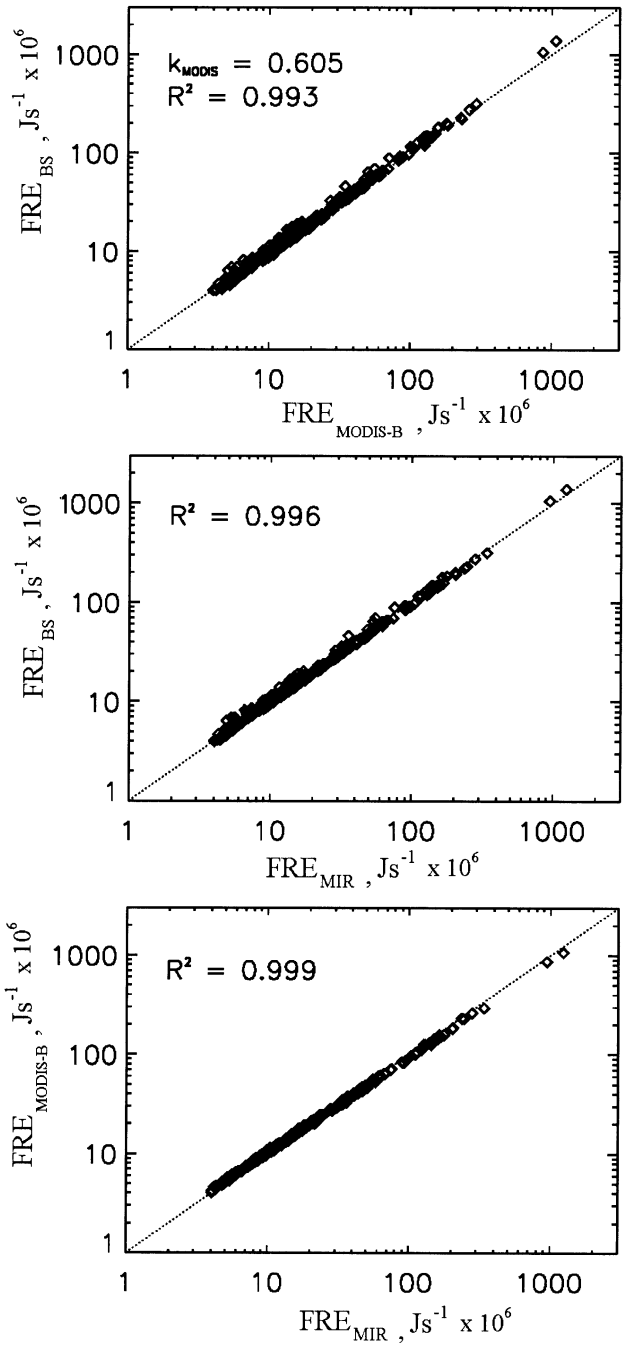

Fig. 18. Relationship between FRE derived via the Bi-spectral method, the MODIS method adapted to BIRD (MODIS-B), and the MIR radiance method for the 319 'reference' clusters selected from the BIRD hotspot pixels of Fig. 15, where FRE_{BS} variability did not exceed 30% as the assumed background temperature was varied around $\bar{L}_{\text{TIR,bg}}\pm\sigma_{\text{TIR,bg}}$.

the MODIS-B and MIR methods are well adjusted to the temperature distribution of the Australian fires. Furthermore, although our simulations indicate that, for example, the MODIS-B method is not well suited to the analysis of fires filling very large proportions of the pixel (Fig. 9) and that the MIR radiance method underestimates FRE at cooler fires (Fig. 13), the strong agreement FRE between the techniques seen in Fig. 18 suggests that the extreme conditions that caused divergence within the simulations do not exist in these particular wildfires.

5.3. BIRD and MODIS FRE intercomparison

The near-simultaneously recorded BIRD and MODIS data were used to intercompare the FRE retrievals made using the two sensors at the same fires. This is the first time such a comparison has been made for FRE observations made by different spaceborne instruments of widely differing spatial resolution and spectral coverage.

Analysis was based on the ten hot clusters of Fig. 17c and d, the MODIS clusters each containing between 1 and 5 contiguous hotspot pixels and the corresponding BIRD clusters between 4 and 126 hot pixels. As can be seen from the figure, many of the BIRD clusters extend spatially beyond the corresponding MODIS cluster, whilst MODIS clusters 4, 6, and 7 cover two or three separate BIRD clusters. In these latter cases, data from the relevant BIRD clusters were combined for comparison to MODIS.

Prior to derivation of FRE, the MODIS and BIRD infrared spectral radiances obtained from each hot cluster were atmospherically corrected to provide estimates of surface leaving spectral radiance in each waveband. Atmospheric correction was performed using MODTRAN 3.7 (Berk, Bernstein, & Robertson, 1989), parameterised using radiosonde data from Sydney Airport taken 3.5 h after the satellite overpass. Atmospheric transmittance and path radiance were calculated at the viewing zenith angle of each sensor relevant to the data of Fig. 17 (MODIS = 26°, BIRD = 0°). Results are shown in Fig. 19, which also indicates the widely differing spectral coverage of the HSRS and MODIS MIR channels used for fire analysis. The Bi-spectral technique was applied to the selected hot clusters and the values of effective fire temperature (T_{EF}) ranged from 740 to 1200 K. The retrieval stability of these temperatures was checked in the same way as was the stability of the FRE estimation, by varying the TIR background radiance around its assumed value $\bar{L}_{TIR,bg}$ in the range of $\pm\sigma_{TIR,bg}$ (Section 5.2). The uncertainty range of the retrieved temperatures was in all cases a maximum of a few hundred Kelvin, making differentiation between flaming and smouldering combustion unreliable, but in all cases the lower bound of T_{EF} (corresponding to the assumed value for the TIR background radiance of $\bar{L}_{TIR,bg} - \sigma_{TIR,bg}$) was higher than 600 K. This proves that the selected fire fronts (1) correspond to active burning and are not just cooling activity and (2) meet the T_{EF} criterion we have defined for the application of the MIR radiance and MODIS-B methods of FRE retrieval.

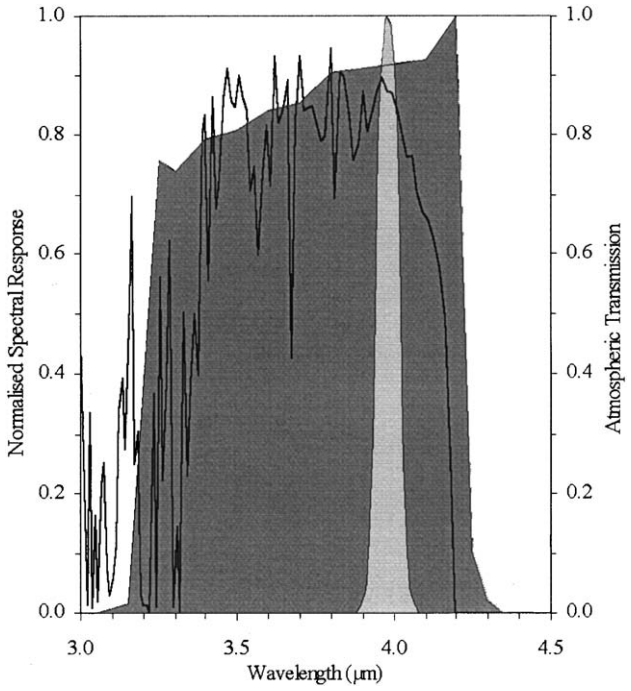

Fig. 19. Atmospheric transmission (solid line) over the MIR wavelength range corresponding to the BIRD (dark grey) and MODIS (light grey) wavebands used for FRE derivation. Atmospheric transmission was calculated via MODTRAN, parameterised with radiosonde data from Sydney Airport, with aerosol characteristics specified using the standard rural model (vis = 23 km). The significant bandpass difference in the HSRS MIR and MODIS band 21 spectral channels is clearly evident, leading to a marked divergence in overall band-weighted atmospheric transmission (0.66 and 0.84, respectively).

The results of applying the various FRE derivation methods to the BIRD and MODIS data of each hot cluster are listed in Table 4, whilst the values derived from application of the MIR radiance method to each sensor are also compared graphically in Fig. 20. As expected from the relationships discussed in Section 5.2 and the data of Fig. 18, estimates of FRE release agree very well for the different FRE retrieval methods applied to data from the same sensor, with variations of +14% to −11% for BIRD and +8% to −8% for MODIS. For the FRE intercomparison between the sensors, in the cases when the MODIS and BIRD clusters cover approximately the same area (clusters 1, 4, 5, 7, and 8), the BIRD and MODIS derived FRE estimates differ by relatively small amounts (within ±15%). However, where clusters are significantly more spatially extended in the BIRD data than in the MODIS data (clusters 2, 3, 6, 9, and 10), the MODIS-derived FRE is significantly lower than the BIRD-derived value, in one case by 46% (Fig. 20). MODIS underestimates FRE in these instances because the fire detection algorithm currently used for the MOD 14 product has failed to identify some active fire pixels within the MODIS data, and as discussed previously this is primarily because of the large spatial resolution of the

Table 4
FRE release of the 10 hot clusters detected in the near-simultaneous MODIS and BIRD data shown in Fig. 15, calculated via the Bi-spectral method, the (adapted) MODIS method, and the MIR radiance method

Hot cluster number (Fig. 15)	MODIS data		BIRD data				
	Fire radiative energy release (J $s^{-1} \times 10^6$)		Fire radiative energy release (J $s^{-1} \times 10^6$)			Estimated fire front length (km)	Estimated fireline intensity (kJ s^{-1} m^{-1})
	MODIS method	MIR radiance method	Bi-spectral method	MODIS-B method	MIR radiance method		
1	165	164	140	132	141	2	70
2	88	86	153	139	158	2	75
3	134	132	210	203	212	3	70
4	28	26	21	23	22	–	–
5	10	9	9	10	9	–	–
6	328	353	396	373	420	6	65
7	213	214	182	157	174	3	60
8	80	78	54	55	57	2	30
9	30	29	34	35	33	2.5	15
10	184	182	246	259	265	9	30

When applied to MODIS data the Bi-spectral method gave unstable results, a finding that agrees with the theoretical study of Giglio and Kendall (2001), and these retrievals are therefore not reported.

sensor when compared to the fire activity. These 'missed' pixels are thus excluded from the FRE computation, leading in these cases to an underestimate of FRE in comparison to the higher spatial resolution BIRD data (which detects a greater proportion of the fire pixels). It should also be noted that a further underestimate of 10–15% in the MODIS-derived FRE values would have been recorded for all clusters had the MODIS data not been atmospherically corrected prior to FRE derivation.

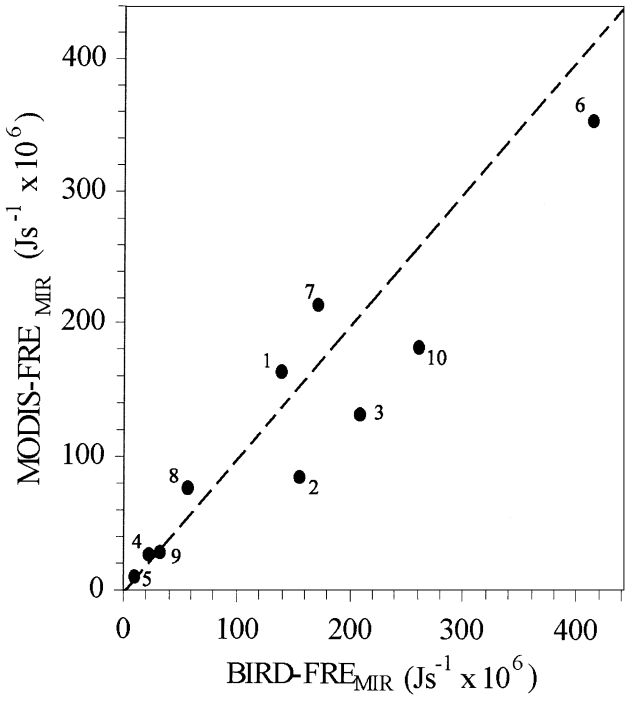

Fig. 20. Comparison of fire radiative energies derived via the MIR radiance method applied to the MODIS and BIRD data of the Sydney fires, shown in Fig. 17. Data labels correspond to those of the hot clusters shown in Fig. 17 and the 1:1 line of agreement is shown.

With the exception of clusters 4 and 5, all the hot clusters detected in the BIRD data show a spatially elongated structure typical of fire fronts. The length of each fire front was estimated from the HSRS data and allows calculation of the mean fire radiative energy release per meter of the fire front. This 'radiative' fireline intensity is a useful parameter, both in terms of helping to direct fire-fighting operations if data are available in near real-time, but also for estimating the effects of the fire on the land surface. Fireline intensity can be calculated from the output of many standard wildfire propagation models (Asensio & Ferragut, 2002; Perry, 1998), making its estimation via BIRD of potential use in the validation of such models. However, it should be recognised that this remotely sensed 'radiative' fireline intensity is derived from a measurement of emitted energy only, rather than the complete heat loss that is predicted in wildfire propagation models, and so comparison of the measured and modelled values must be undertaken with caution. For the selected fronts of the Sydney fires, radiative fireline intensity estimated from BIRD varied between 15 and 75 kJ s^{-1} m^{-1}, substantially lower than the values usually assumed for intense wildfires of this sort via the standard modelling approach (Byram, 1959). Wooster, Perry, Zhukov, and Oertel (2003) discuss some of the possible reasons for differences between the measured and modelled values, including substantial convective energy losses not accounted for in the radiatively derived measurement and the frequent but potentially inaccurate modelling assumption that complete (100%) combustion occurs. Interestingly, the magnitude of the difference between the measured 'radiative' and modelled 'total' values of fireline intensity appears to be around the same order as that between the measured amount of radiative heat emitted per unit mass of vegetation (Wooster, 2002) and the theoretical total 'heat yield' parameter used in modelling (Byram, 1959). Replacement of the theoretical heat-yield parameter by the measured 'radiative heat yield' may there-

fore be appropriate when using models to interpret remotely sensed values of fireline intensity and studies are continuing on this issue. Estimation of radiative fireline intensity is not possible from MODIS since this lower spatial resolution sensor detects only small groups of hot pixels, rather than complete fire fronts.

The total FRE release in the BIRD and MODIS image fragments of 5 January shown in Fig. 17 was calculated as 2.5 and 1.3×10^9 J s^{-1}, respectively. Similarly, the total FRE release in the entire coverage of that date (Figs. 15b and 16), including all hot clusters detected by BIRD, was 6.5×10^9 J s^{-1} from BIRD (actually in the uncertainty range 6–8.3 J s^{-1} using $\bar{L}_{TIR,bg} \pm \sigma_{TIR,bg}$; Table 3) and 4.0×10^9 J s^{-1} from MODIS. Thus, MODIS again underestimates the total fire radiative energy release in comparison to BIRD, due to its inability to detect the lower intensity fire pixels. Though the FRE release of each of these individual undetected fires is small, their relatively large number makes their overall FRE significant.

6. Estimation of 'active fire' FRE and the effect of cooling ground

Wooster (2002) explored the relationship between the mass of vegetation combusted in small-scale experimental burns and the FRE released as measured by ground-based spectro-radiometry. The ultimate aim is to provide parameters that would allow biomass combustion rates to be derived from FRE observations made by airborne and spaceborne sensors. However, in these ground-based observations, the fires filled a large proportion of the radiometer field-of-view and were confined to one area rather than progressing over the landscape as would a natural wildfire, so were assumed to consist of flaming and smouldering components only. The results of Wooster (2002) suggest that FRE from these components can indeed be related to rates of biomass combustion, but the ground-based measure of FRE is somewhat different to the satellite-derived FRE retrievals considered in this paper since the latter includes an additional FRE contribution from any cooling ground exposed within the pixel. A comparison of FRE retrievals that include and exclude the cooling ground component is therefore required to consider the applicability of ground-based FRE-to-biomass combustion rate relationships to satellite-derived FRE observations.

Table 2 includes details of the true FRE release from each of the three fire components considered during the simulations described in Section 4. Since the true FRE of the cooling component is an order of magnitude smaller than that of the smouldering component and two orders of magnitude smaller than that of the flaming component, its inclusion or exclusion in the derivation of FRE will only be highly critical for pixels, clusters or regions where the area of cooling ground is very large in comparison to that of the active fire. Furthermore, the MIR and MODIS-B methods always suppress the effect of the cooling component on FRE derivation via their substantial underestimation of it, as can be seen in Figs. 10–13 and the ~ order of magnitude underestimates shown in Table 2. This suggests that in cases where substantial cooling ground is exposed to the sensor, satellite-derived FRE calculated via the MIR and MODIS-B methods will be more representative of FRE emitted from the flaming and smouldering components only (which we

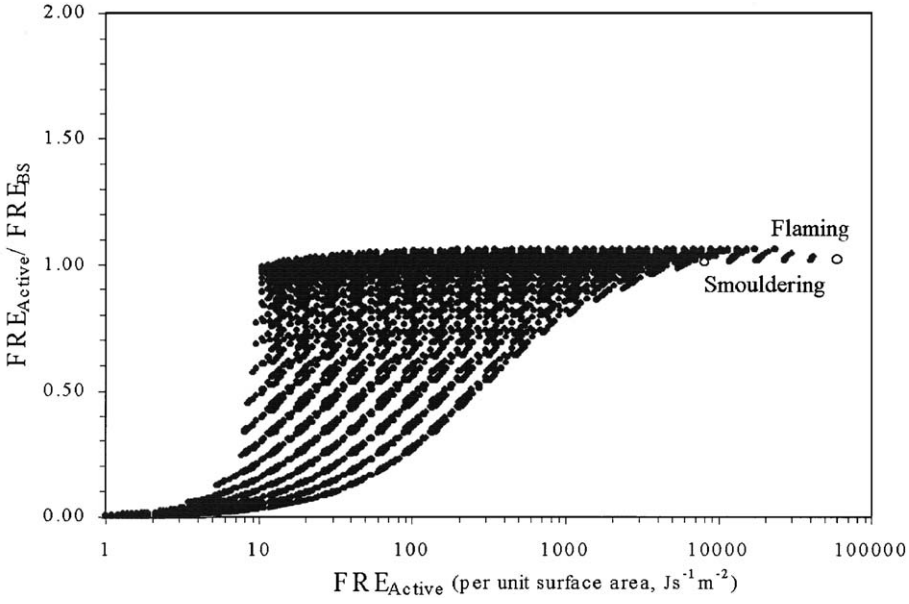

Fig. 21. Ratio of FRE from the active fire (flaming and smouldering) components only (FRE_{Active}) to the total FRE estimated via the Bi-spectral technique for the non-homogeneous fire model. Open circles represent the separate flaming and smouldering active fire components covering 100% of area (with the gaussian temperature distributions shown in Table 2), whereas the dots represent mixtures of these, cooling ground, and the ambient temperature background. Note that actual active fire FRE (*x*-axis) is here expressed per unit area of the surface, only some of which will be covered by fire.

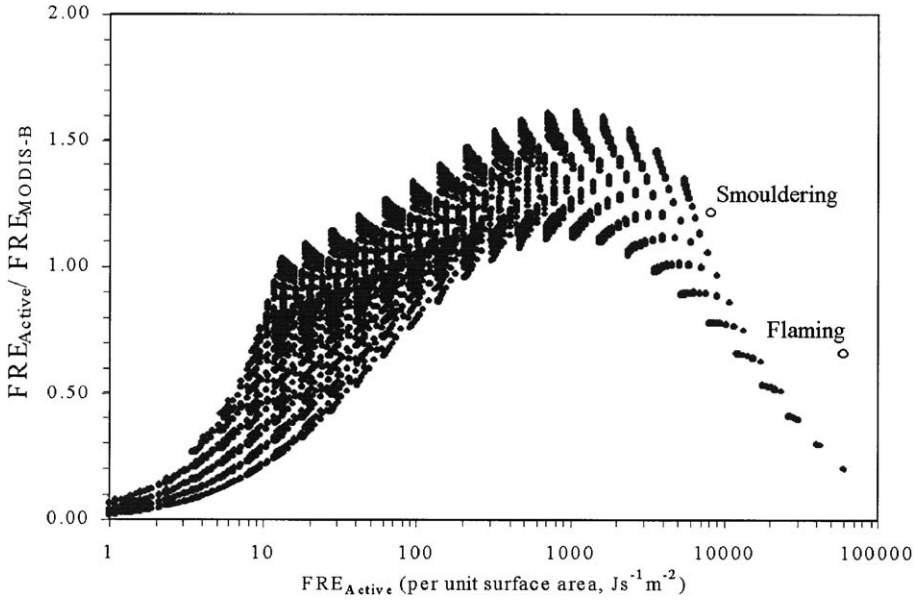

Fig. 22. Ratio of FRE from the active fire (flaming and smouldering) components only (FRE_{Active}) to the total FRE estimated via the MODIS-B method for the non-homogeneous fire model. Open circles represent the separate flaming and smouldering active fire components covering 100% of area (with the gaussian temperature distributions shown in Table 2), whereas the dots represent mixtures of these, cooling ground, and the ambient temperature background. Note that actual active fire FRE (*x*-axis) is here expressed per unit area of the surface, only some of which will be covered by fire.

here term FRE_{Active}) than will FRE calculated by the Bi-spectral method. Thus, the MIR and MODIS-B methods may actually be advantageous in this respect.

We have used the non-homogeneous fire model to check this supposition and to investigate the exact extent to which the FRE retrieved via the three methods tested can actually be considered representative of FRE_{Active}. The results confirm that when FRE_{Active} is small and the contribution from cooling ground dominates, then FRE_{MIR} and $FRE_{MODIS\text{-}B}$ are significantly closer to FRE_{Active} than is FRE_{BS}. For example, FRE_{Active} must exceed $\sim 700\ J\ s^{-1}\ m^2$ for the ratio $(FRE_{Active})/(FRE_{BS})$ to reach 0.7 (Fig. 21), whilst FRE_{Active} needs only to exceed $\sim 100\ J\ s^{-1}\ m^2$ to for the ratios $(FRE_{Active})/(FRE_{MODIS\text{-}B})$ and $(FRE_{Active})/(FRE_{MIR})$ (Figs. 22 and 23) to exceed the same 0.7 threshold. It can also be seen

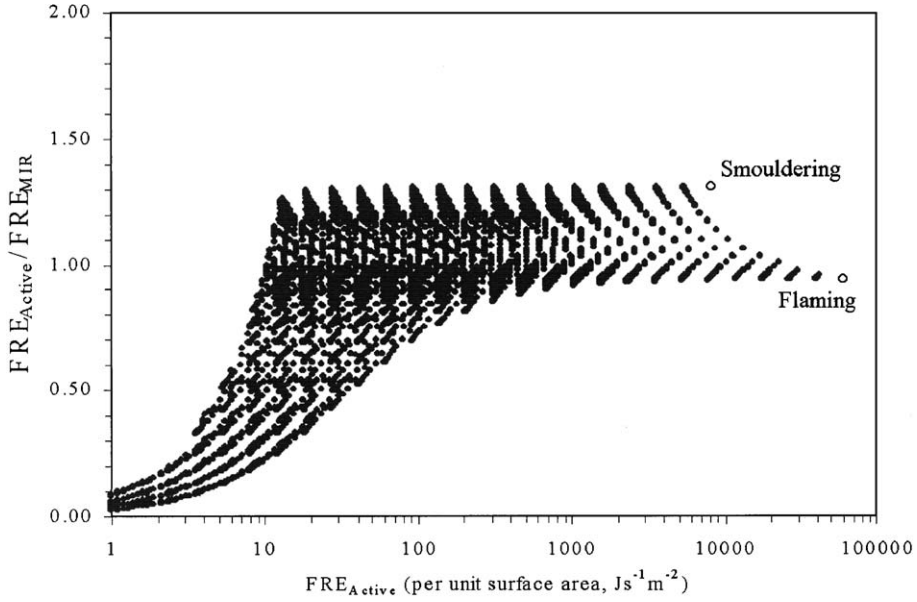

Fig. 23. Ratio of FRE from the active fire (flaming and smouldering) components only (FRE_{Active}) to the total FRE estimated via the MIR radiance method for the non-homogeneous fire model. Open circles represent the separate flaming and smouldering active fire components covering 100% of area (with the gaussian temperature distributions shown in Table 2), whereas the dots represent mixtures of these, cooling ground, and the ambient temperature background. Note that actual active fire FRE (*x*-axis) is here expressed per unit area of the surface, only some of which will be covered by fire.

that at higher values of FRE_{Active} (>1000 J s^{-1} m^2) the ratio $(FRE_{Active})/(FRE_{MODIS\text{-}B})$ begins to fall strongly (Fig. 22) due to the MODIS-B methods overestimation of total FRE when a fire occupies a large pixel proportions (Fig. 10). This fall is not seen in the case of the MIR radiance method, for which the ratio $(FRE_{Active})/(FRE_{MIR})$ lies consistently within the range 0.7–1.3 in the FRE_{Active} range 100–100,000 J s^{-1} m^2 (Fig. 23).

7. Conclusion

The remote measurement of fire radiative energy was first proposed by Kaufman, Justice, et al. (1998), Kaufman, Kleidman, et al. (1998), and Kaufman et al. (1996) as a novel method for providing information on variations in the amount of biomass consumed per unit time in vegetation fires, theoretically allowing the total amount of biomass combusted to be derived if sufficient observations of FRE are available (Wooster, 2002). Until recently, only the MODIS sensor of the EOS Terra (and now Aqua) satellites possessed the necessary spectral and radiometric characteristics suitable for providing FRE observations from low-Earth orbit (Kaufman, Justice, et al., 1998). The HSRS sensor of the new experimental BIRD satellite now allows FRE derivation at high spatial resolution and for fires of a smaller size and intensity than does MODIS, albeit at a much lower revisit time.

In this paper, we have demonstrated the physical reason why the amount of energy radiated by an active fire over all wavelengths can be estimated by analysing emission in only the MIR spectral region or, in the case of the Bi-spectral method, the MIR and TIR regions. We have discussed the existing Bi-spectral and MODIS methods to derive FRE and have adapted them for use with BIRD. We have also illustrated an alternative method to derive FRE, based on MIR spectral radiances, and determined the coefficients appropriate for the application of this method to both BIRD and MODIS data. Amongst these three approaches, only the Bi-spectral method provides an adaptation to fire temperature and its use is recommended in cases when it proves to be stable to temperature uncertainties in the TIR background. Such uncertainties typically prevent the accurate application of the method to data from moderate resolution sensors like MODIS, but the method works well for larger fires analysed via the higher spatial resolution BIRD-HSRS imager. For FRE analysis via MODIS, or for fires analysed by BIRD where the Bi-spectral retrievals appear unstable due to a small fire size or a highly variable 'ambient' background, use of the MODIS or MIR radiance methods is recommended. These methods also offer the potential advantage that they can be applied to single pixels, rather than pixel clusters, since they are unaffected by sensor multiband mis-registration effects.

Our simulations indicate that the MIR radiance and MODIS methods are applicable when the effective fire temperature (i.e., T_{EF}, the effective temperature of the subpixel emitter that would provide the observed MIR and TIR signal) is greater than 600 K. Furthermore, the MIR radiance method potentially provides a higher accuracy than the MODIS method when T_{EF} rises above ~ 700 K (Figs. 11 and 13) and unlike the MODIS method it appears broadly applicable to both small and large fires. Thus, the MIR radiance method may be optimal for higher-temperature fires and also newly active volcanic lavas. The MODIS method is best suited to fires that are much smaller than the pixel area, as is the expected case when using the technique with MODIS rather than BIRD data; and indeed the MODIS method algorithm was originally optimised for this situation. Simulations indicate that the MODIS method is also best suited to the analysis of lower temperature fires, dominated by smouldering combustion.

Both the MIR radiance and MODIS methods can strongly underestimate total fire radiative energy release at the lowest temperature fires considered (< 600 K). This fact, coupled with the instability of the Bi-spectral method when applied to fires providing a small TIR signal, means that the case of smaller, cooler fires is likely to provide the most difficult situation for reliable FRE retrieval. However, since these fires will also provide the lowest FRE values, they will typically be combusting much smaller amounts of biomass than more intensely burning, higher-temperature events.

When BIRD and MODIS are used to retrieve FRE for the January 2002 Sydney fires, the three FRE derivations methods provide excellent agreement when using data from the same instrument, suggesting that the characteristics of these real fires did not include the extreme conditions that caused FRE retrievals made by each method to diverge during the simulation studies. Detailed comparison between the BIRD and MODIS retrievals of individual fires indicates that MODIS underestimates FRE at half the fires examined (by up to 46%), largely due to some of the fire-affected pixels being detected by BIRD but not by the lower spatial resolution MODIS. However, for the remaining fires very similar FRE values were obtained from each sensor despite the marked difference in MIR band spectral coverage and sensor pixel size, again indicating the robustness of the method and its suitability for use with data of different spatial resolutions. This provides additional confidence in the reliability and merit of remotely sensed FRE observations made from low-Earth orbit and we echo the suggestion of Kaufman, Justice, et al. (1998) and Kaufman, Kleidman, et al. (1998) that the technique appears highly promising for enhancing studies of biomass burning rates, emissions and total vegetation loss. Further simulations indicate that, since the MODIS and MIR methods underestimate the FRE contribution from cooling ground when compared to the Bi-spectral method, they may actually show some advantages when attempting to use satellite data to retrieve estimate of the FRE contribution from the active fire (flaming and smouldering) components only. The MIR radiance method appears particularly strong in this regard,

allowing FRE_{Active} to be estimated to within ±30% in the FRE_{Active} range 100–100,000 J s^{-1} m^2. Future intercomparisons between simultaneously recorded BIRD and MODIS data may allow MODIS-derived FRE to be 'calibrated' against the more accurate BIRD-derived values. It is important however, that such a comparison be carried out separately for each fire-prone ecosystem, and with appropriate regard to any changes in fire characteristic that occur over the 'fire' season. This is because the characteristics of fire size and temperature, to which the FRE retrieval methods are somewhat sensitive, varies with environmental condition (Belward, Kennedy, & Grégoire, 1994), as does the likely success rate of the MODIS fire detection algorithm with respect to that of BIRD. These variations may have significant impacts on the ratio of MODIS to BIRD-derived FRE made under different conditions.

Results from this study lead us to expect that FRE will become an important tool for enhancing global studies of terrestrial vegetation fires with infrared remote sensing, particularly as the majority of large fires are now observed four times per day via the Terra and Aqua MODIS instruments. In addition to further MODIS-BIRD intercomparisons for different fire prone ecosystems, and study of the global distribution of FRE via MODIS to better determine the extent of potential FRE underestimation due to the presence of cooler fires, one key point that remains to be determined is the extent to which the 'snapshots' available from polar orbiting platforms are able to characterise temporal variations in FRE. This maybe examined via comparison to geostationary MIR radiance data such as that from the GOES and Meteosat Second Generation imagers and Wooster et al. (in press) show the first case of FRE derivation from a geostationary platform. A further point is that, whilst the FRE technique is largely insensitive to smoke due to its relative transparency at MIR wavelengths, meteorologic cloud cover will hamper FRE observations. Whilst clouds are, perhaps, less frequent in many areas during the 'dry' seasons that are usually associated with fire activity, they will still prevent observation of FRE in many cases. We therefore expect that some combination of FRE analysis and post-fire burn scar mapping will be required to tackle this limitation.

Acknowledgements

MODIS data were obtained via the NASA Goddard Space Flight Center (GSFC) and EROS Data Centre Distributed Active Archive Centers (DAACs). We are grateful to Louis Giglio for advice regarding the use of the MODIS Fire Products and to the BIRD team of the German Aerospace Center (DLR) for providing the high-resolution fire data. M. Wooster holds a NERC Earth Observation Science Initiative lectureship, and this work was supported in part by NERC grant NER/Z/S/2001/01027. We are very appreciative of the three anonymous referees for their thoughtful and constructive comments that helped us improve the clarity and content of this paper.

References

Andreae, M., & Merlet P. (2001). Emissions of trace gases and aerosols from biomass burning. *Global Biogeochemical Cycles*, *15*(4), 955–966.

Asensio, M. I., & Ferragut, L. (2002). On a wildland fire model with radiation. *International Journal for Numerical Methods in Engineering*, *54,* 137–157.

Belward, A. S., Kennedy, P. J., & Grégoire, J. -M. (1994). The limitations and potential of AVHRR GAC data for continental scale fire studies. *International Journal of Remote Sensing*, *15*, 2215–2234.

Berk, A., Bernstein, L. S., & Robertson, D. C. (1989). MODTRAN: a moderate resolution model for LOWTRAN 7. Final Report GL-TR-89-0122, Geophysics Laboratory, U.S. Air Force Systems Command, Hanscomb AFB, MA, USA.

Briess, K., Jahn, H., Lorenz, E., Oertel, D., Skrbek, W., & Zhukov, B. (2002). Fire recognition potential of the Bi-spectral InfraRed Detection (BIRD) satellite. *International Journal of Remote Sensing* (in review).

Byram, G. M. (1959). Combustion of forest fuels. In K. P. Davis (Ed.), *Forest fires: control and use* (pp. 65–89). New York: McGraw Hill.

Crutzen, P., & Andreae, M. (1990). Biomass burning in the tropics: impact on atmospheric chemistry and biogeochemical cycles. *Science*, *250*, 1669–1678.

Dozier, J. (1981). A method for satellite identification of surface temperature fields of sub-pixel resolution. *Remote Sensing of Environment*, *11*, 221–229.

Fuller, D. (2000). Satellite remote sensing of biomass burning with optical and thermal sensors. *Progress in Physical Geography*, *24*, 543–561.

Giglio, L., & Kendall, J. D. (2001). Application of the Dozier retrieval to wildfire characterization—a sensitivity analysis. *Remote Sensing of Environment*, *77*, 34–49.

Hirsch, S. N., Kruckeberg, R. F., & Madden, F. H. (1971). The bi-spectral forest fire detection system. *Proceedings of the 7th international symposium on remote sensing of environment, 17–21 May 1971* (pp. 2253–2272). Ann Arbor: Environmental Research Institute of Michigan.

Justice, C. O., Giglio, L., Korontzi, S., Owens, J., Morisette, J. T., Roy, D., Descloitres, J., Alleaume, S., Petitcolin, F., & Kaufman, Y. (2002). The MODIS fire products. *Remote Sensing of Environment*, *83*, 244–262.

Kaufman, Y., & Justice, C. (1998). *MODIS Fire Products, Algorithm Theoretical Basis Document, Version 2.2, MODIS Fire Team (EOS ID#2741)* (p. 77).

Kaufman, Y., Remer, L., Ottmar, R., Ward, D., Rong-R, L., Kleidman, R., Fraser, R., Flynn, L., McDougal, D., & Shelton, G. (1996). Relationship between remotely sensed fire intensity and rate of emission of smoke: SCAR-C experiment. In J. Levine (Ed.), *Global biomass burning* (pp. 685–696). MA: MIT Press.

Kaufman, Y. J., Justice, C. O., Flynn, L. P., Kendall, J. D., Prins, E. M., Giglio, L., Ward, D. E., Menzel, W. P., & Setzer, A. W. (1998). Potential global fire monitoring from EOS-MODIS. *Journal of Geophysical Research*, *103*, 32215–32238.

Kaufman, Y. J., Kleidman, R. G., & King, M. D. (1998). SCAR-B fires in the tropics: properties and remote sensing from EOS-MODIS. *Journal of Geophysical Research*, *103*, 31955–31968.

Kaufman, Y. J., Tucker, C. J., & Fung, I. (1990). Remote sensing of biomass burning in the tropics. *Journal of Geophysical Research*, *95*, 9927–9939.

Langaas, S. (1995). *A critical review of sub-resolution fire detection techniques and principles using thermal satellite data.* PhD Thesis, Department of Geography, University of Oslo, Norway.

Lorenz, E., & Skrbek, W. (2001). Calibration of a Bi-spectral Infrared Push-Broom Imager. *Proceedings of SPIE, Infrared Spaceborne Remote Sensing IX, San Diego, 29 July–3 August 2001*, in press.

Matson, S., Schneider, S. R., Aldridge, B., & Satchwell, B. (1984). *Fire detection using the NOAA-series satellites*. Washington, DC: National Oceanic and Atmospheric Administration. NOAA Technical Report NESDIS 7.

Nishihama, M., Wolf, R., Solomon, D., Patt, F., Blanchette, J., Fleig, A., & Masouka, E. (1997). *MODIS level 1A earth location: algorithm theoretical basis document version 3.0*. Maryland, USA: NASA Goddard Spaceflight Centre, 147pp.

Pereira, J. M. C., Pereira, B. S., Barbosa, P., Stroppiana, D., Vasconcelos, M. J. P., & Gregoire, J. M. (1999). Satellite monitoring of fire in the EXPRESSO study area during the 1996 dry season experiment: active fires, burnt area, and atmospheric emissions. *Journal of Geophysical Research*, *104*, 30701–30712.

Perry, G. L. W. (1998). Current approaches to modelling the spread of wildland fire: a review. *Progress in Physical Geography*, *22*, 222–245.

Prins, E. M., Feltz, J. M., Menzel, W. P., & Ward, D. E. (1998). An overview of GOES-8 diurnal fire and smoke results for SCAR-B and 1995 fire season in South America. *Journal of Geophysical Research*, *103*, 31821–31835.

Robinson, J. M. (1991). Fire from space: global fire evaluation using infrared remote sensing. *International Journal of Remote Sensing*, *12*, 3–24.

Scholes, M., & Andreae, M. O. (2000). Biogenic and pyrogenic emissions from Africa and their impact on the global atmosphere. *Ambio*, *29*, 23–29.

Skrbek, W., & Lorenz, E. (1998). HSRS—an infrared sensor for hot spot detection. *Proceedings of SPIE Infrared Spaceborne Remote Sensing VI*, *3437*, 167–176.

Spichtinger, N., Wenig, M., James, P., Wagner, T., Platt, U., & Stohl, A. (2001). Satellite detection of a continental-scale plume of nitrogen oxides from boreal forest fires. *Geophysical Research Letters*, *28*, 4579–4582.

Waggoner, J. (1991). Airborne system locates fires. *Photonics Spectra*, *25*, 22.

Wittenberg, U., Heimann, M., Esser, G., McGuire, A., & Sauf, W. (1998). On the influence of biomass burning on the seasonal CO_2 signal as observed at monitoring stations. *Global Biogeochemical Cycles*, *12*, 531–544.

Wooster, M. J. (2001). Long-term infrared surveillance of Lascar Volcano: contrasting activity cycles and cooling pyroclastics. *Geophysical Research Letters*, *28*, 847–850.

Wooster, M. J. (2002). Small-scale experimental testing of fire radiative energy for quantifying mass combusted in natural vegetation fires. *Geophysical Research Letters*, *29*(21), 2027 (doi: 10.1029/2002GL015487).

Wooster, M. J., Perry, G., Zhukov, B., & Oertel, D. (2003). Estimation of energy emissions, fireline intensity and biomass consumption in wildland fires: a potential approach using remotely sensed fire radiative energy. In R. Kelly, N. Drake, & S. Barr (Eds.), *Spatial modelling of the terrestrial environment*. London: Wiley, in press.

Wooster, M. J., & Rothery, D. A. (1997). Thermal monitoring of Lascar Volcano, Chile using infrared data from the Along Track Scanning Radiometer: a 1992–1995 time-series. *Bulletin of Volcanology*, *58*, 566–579.

Zhukov, B., & Oertel, D. (2001). Hot spot detection and analysis algorithm for the BIRD mission. Algorithm Theoretical Basic Document, DLR-Berlin.